



Depósito de investigación de la Universidad de Sevilla

<https://idus.us.es/>

Esta es la versión aceptada del artículo publicado en:

This is an accepted manuscript of a paper published in:

Automation in Construction (2021): 30/1/2024

**DOI:** <https://doi.org/10.1016/j.autcon.2021.103856>

**Copyright:** © 2021 Elsevier B.V. All rights reserved.

El acceso a la versión publicada del artículo puede requerir la suscripción de la revista.

Access to the published version may require subscription.

“This is an Accepted Manuscript of an article published by Elsevier in [Automation in Construction] on [2021], available at : <https://doi.org/10.1016/j.autcon.2021.103856>.”

”

1 **Title**

2 Semantic interpretation of architectural and archaeological geometries: Point cloud  
3 segmentation for HBIM parameterisation

4 **Author names and affiliations**

5 Juan Moyano<sup>1\*</sup>, Javier León<sup>1</sup>, Juan E. Nieto-Julián<sup>1</sup> and Silvana Bruno<sup>3</sup>

6 <sup>1</sup> Departamento de Expresión Gráfica e Ingeniería en la Edificación, Escuela Técnica Superior  
7 de Ingeniería de Edificación, Universidad de Sevilla, 4A Reina Mercedes Avenue, Seville  
8 41012, Spain.

9  
10 <sup>3</sup> Politécnico de Bari, Department of Civil, Environmental, Land, Building Engineering and  
11 Chemistry (DICATECh), Via Edoardo Orabona, 4, 70125 Bari, Italia

12 <https://doi.org/10.1016/j.autcon.2021.103856>

13 **Abstract**

14 The creation of Cultural Heritage (CH) Digital Twins is based on i) the capture of geometric data  
15 using digital technologies (laser scanning and photogrammetry); ii) the processing of the raw  
16 data to identify, segment and label the objects; and iii) their conversion into BIM objects.  
17 Hitherto, the most extensive method for BIM segmentation and modelling is manual, which  
18 led to research into the automation of this process, also in the field of CH. Manual operations  
19 are still labour-intensive and mathematical approaches are not inclusive for all CH specialists.  
20 In this context, this research studies the application of Brodu and Lague's morphological  
21 segmentation algorithm called CANUPO to classify the architectural components of the façade  
22 of the 16th-century Casa de Pilatos Palace in Seville, Spain, from a Terrestrial Laser Scanning  
23 (TLS) point cloud dataset. In this paper, the experimentation on semantic segmentation was  
24 carried out using open-source software, specifically the CANUPO algorithm integrated into  
25 CloudCompare software.

26 **Keywords**

27 Historic Building Information Modelling (HBIM), automatic segmentation, laser scanning and  
28 photogrammetry, segmentation algorithm CANUPO.

29 **Introduction**

30 In recent times, 3D modelling has received special attention in the Archaeological and  
31 Architectural Heritage field. The models must contain precise construction characteristics to be  
32 representative of Cultural Heritage (CH) reality. For this purpose, data acquisition techniques  
33 that allow Building Information Modelling (hereinafter, BIM) software to build geometries  
34 from point clouds are used. Modelling the CH requires completeness and accuracy, which are  
35 necessary for comprehensive representation. Therefore, the use of massive data capture  
36 techniques such as Structure-from-Motion/Multi-View-Stereo (SfM/MVS) and Terrestrial Laser  
37 Scanning (TLS) is increasingly being adapted to a BIM process applied to heritage. This allows  
38 Digital Twins to be exported to BIM platforms for parametric modelling. However, the BIM  
39 representation is a complicated and resource-intensive process when the built elements  
40 belong to CH. The difficulty of modelling existing objects in historic buildings with structural  
41 deformations and complex shapes is still a weakness of the HBIM process [1,2] The new BIM  
42 paradigm relies on the building information model to improve the efficiency of construction

43 operations, maintenance, and the project life cycle. It also becomes a container to record and  
44 catalogue sometimes unexplored information [3].

45 Nevertheless, the problem lies in the automatic segmentation procedures for subsequent  
46 element modelling. This is the case, for example, for complex façades that are common in  
47 architectural heritage, whose SfM or TLS range clouds contain hundreds of million points.  
48 These files are difficult to handle, even for the manual segmentation of the elements. Two  
49 decades ago, when computers were not present in the area of architecture and heritage, the  
50 way of segmenting in traditional drawings was to structure the compositional units of a  
51 historic building façade according to the hierarchy of its elements. With the emergence of the  
52 new BIM paradigm, Murphy et al. [4] were the first to work with parametric models of  
53 Renaissance architecture from point clouds using a cross-platform software system. The work  
54 was conceived as a simple visualisation tool that structured the elements through a grammar  
55 of ornamentation and composition that they called linguistic analogy. The shape grammar can  
56 recognise architectural styles and can be divided into a set of basic shapes. This is the  
57 procedure currently being carried out in semantic segmentation.

58 In recent times, researchers and academics are striving to achieve processes that help  
59 recognise historical architectural features using learning techniques based on Deep Learning  
60 (hereafter DL) [5] at an appropriate level of detail. However, the use of neural networks for  
61 point cloud segmentation may limit the operator usability. Even when undertaking  
62 segmentation by artificial intelligence, point cloud files contain such a large amount of data  
63 that they may not be operational with current hardware and software. It is therefore  
64 necessary to develop new strategies related to the interoperability of accurate modelling  
65 systems [6], and especially those related to data management.

66 In this work, an experimental process was developed to demonstrate the applicability of Brodu  
67 and Lague's algorithm [7]. This was carried out with a TLS point cloud of a façade of the 16th-  
68 century Casa de Pilatos Palace in Seville, Spain. This algorithm, available as a plug-in called  
69 CANUPO in CloudCompare software [8], works as a 3D multiscale classifier by training  
70 elementary binary classifiers.

71 Brodu and Lague developed the system on a natural scene subset to recognise rocks,  
72 vegetation, water, and gravel in a riverbed. However, these authors aimed at experimenting  
73 with the geometric fidelity that semantic segmentation can achieve to classify architectural  
74 elements under the training of this software. These tests have not been applied before; thus,  
75 this is an original methodology. The results are compared with manual segmentation to  
76 evaluate the selected point set and, once the results of the subsets are obtained, the BIM is  
77 created, and the suitability of the data for accurate 3D geometric reconstruction is examined.

## 78 **Literature review**

79 3D reconstruction is the process by which a computer replicates the physical characteristics of  
80 a real object. The shape and appearance of the three-dimensional object or volumetric scene  
81 are recovered by analysing the digital information provided by different types of sensors [9].  
82 Therefore, the main objective is to obtain an algorithm capable of representing the connection  
83 between the point set from data acquisition techniques and transforming it into a surface  
84 shape, be it triangles or any other surface. Applications in the CH field are increasing [10] and  
85 becoming particularly challenging when it comes to establishing the maximum fidelity in the  
86 3D reconstruction [11]. Most studies on parametric element reconstruction from range clouds  
87 focus on the representation of planar surfaces [12], independent elements with no

88 information about their relationships. This means that there is also no relationship between  
89 the elements and their morphology. In this way, to establish a connection between an element  
90 and its function, the first step is to analyse the object shapes and to perform semantic  
91 modelling of the compositional elements (classification of their shapes). An example of  
92 semantic modelling is the work by Gaiani [13] on the Altar of the marble shrine of Augustus.  
93 This analysis determines the simplification degree when the objects are not separate but form  
94 an architectural ensemble. Previous studies addressed the classification of building  
95 components. This classification usually appears as identity coding of architectural elements in  
96 architectural treatises [14] and could be related to the hierarchical description of building  
97 components.

98 The scientific literature has attempted to analyse the geometric quality of the 3D model [15]  
99 by evaluating its accuracy based on the LiDAR survey. Here, the level of detail of the model  
100 depends on the point cloud resolution. However, current digital BIM platforms cannot handle  
101 records with an excessive amount of information in the range clouds. Therefore, it is necessary  
102 to establish the procedures involved in the transformation of these point sets into a Heritage  
103 BIM project (HBIM) and, secondly, to know how these processes can be optimised. When  
104 approaching the modelling of a restoration project, the identification of the geometric  
105 characterisation (architectural morphology) can be articulated around two points of view [14],  
106 the raw processing of the dataset in the digital model and the use of the semantic information  
107 produced by the design model. The former refers to data acquisition processing in the form of  
108 Massive Data Capture Systems (MDCSs), and the latter is supported by a BIM tool; this  
109 methodology aims at creating a digital information system associated with graphic  
110 documentation [16].

111 To solve the transformation of the point cloud into BIM parametric objects, several authors  
112 have reviewed the extensive scientific literature on SfM data [17–21] and TLS point clouds  
113 [15,22–25]. In this sense, the importance of fields of knowledge such as geomatics and 3D  
114 model reconstruction is highlighted. From these efforts to achieve automation of point cloud  
115 to BIM processes, the relatively new term semantic segmentation has emerged. According to  
116 Yang et al. [26], this is a critical issue. The proposed solution is to limit point sets in subset units  
117 whose information can be handled by digital platforms. Thus, Spina et al. [27] used the term  
118 point cloud segmentation as a way to process and organise the point cloud into meaningful  
119 subsets. This organisation makes it possible to reduce the shape complexity of the raw point  
120 cloud and to facilitate the processing of 3D object surveys. The reason the semantic  
121 segmentation is useful is twofold: i) point clouds contain information about the actual  
122 geometry of the object, but lack semantic information on the categories of objects or materials  
123 constituting the building components [28]; ii) point cloud simplification allows to operate in  
124 BIM platforms to implement object geometries. Achieving 3D models requires tasks such as  
125 segmentation which, according to Aitelkadi et al. [29], is the key step during the point cloud  
126 processing to identify homogeneous areas. Thus, most of the segmentation focuses on the  
127 information from the point cloud.

128 The extraction of semantic features was summarised by Pu et al. [30], who determined the  
129 optimal values of the segmentation parameters as size, position, orientation, topology, and  
130 point density. The proposed segmentation is based on point colour, laser intensity, and  
131 geometric data. These strategies involve an automatic identification process without the need  
132 for operator intervention. Boochs et al. [31] defined segmentation as the combination of  
133 algorithms that improve projective reconstruction. Grilli et al. [29] defined it as the process of

134 grouping "point clouds into multiple homogeneous regions with similar properties, while  
135 classification is the step that labels these regions". Classification as outlined by Grilli et al [29]  
136 is based on the need to bring the point cloud into the BIM software through identification. In  
137 other words, the aim is to determine the meaning of function and shape in the 3D elements,  
138 although most segmentation algorithms work with a 2.5D surface model hypothesis [32].

139 Supervised methods require a preceding training phase for the classification solution. Previous  
140 studies focus on identifying vertical elements such as walls, floors, or those limited by floors  
141 [33] or other elements. They can also integrate the knowledge of specific elements into the  
142 point cloud, especially to develop interior elements [28,34,35]. Grilli et al. [29] reviewed and  
143 classified segmentation algorithms as those based on edges [36] and data [37], region growing  
144 segmentation[36], or model fitting segmentation based on point fitting using RANSAC  
145 programming [27,38]. An approach based on decomposing architectural structures into  
146 geometric primitives (planes, cylinders and spheres) might seem suitable for their  
147 mathematical adjustment via parametric object modelling (BIM) algorithms. However, the use  
148 of these algorithms is sometimes not within the reach of regular BIM operators. The reason for  
149 this lies in the software usability, which requires mathematical processes; secondly, because  
150 not all point cloud files are valid since they may or may not be structured. Most segmentation  
151 algorithms work with structured or LiDAR files.

## 152 **Generation of geometric construction models**

153 Newly constructed buildings respond to a project theory based on volumes, new materials and  
154 forms of construction. On the contrary, the built CH (historic buildings) is the result of  
155 numerous transformations over time and is subject to building components constructed at  
156 various periods depending on the refurbishment carried out.

157 The generation of parametric as-built 3D models from massive data acquisition is a reality for  
158 complex surfaces of historic buildings. Over time, several attempts have been made at semi-  
159 automatic methods that allow the creation of parametric models from point clouds [39],  
160 focusing on model accuracy [40]. Other approaches use curves and NURBS surfaces to  
161 reconstruct complex objects [41] without oversimplification. The advantage of creating  
162 parametric objects on digital BIM platforms is that the resulting products are dynamic objects  
163 that can be transformed instantaneously [42]. However, this process is ideal for  
164 reconstructions where the objects are ideal models from architectural manuals or libraries  
165 within specific software. The complexity of historic architecture goes beyond this. Therefore,  
166 parametric 3D reconstruction from digital twins captured by TLS or SfM is a knowledge gap.  
167 The aim is that both architectural and archaeological elements modelled on digital platforms  
168 should represent the greatest geometric similarity to real objects, essentially to preserve their  
169 characteristic geometric uniqueness.

170 The model associated with the structure ensemble offers the opportunity to relate the  
171 accuracy of the HBIM to the level of detail (LOD) needed. To do this, some researchers [43]  
172 used various workflows based on mathematical algorithms, such as software applications  
173 including Rhino-Grasshopper [39] and Dynamo [44], which interact with programmes such as  
174 Graphisoft ArchiCAD or Autodesk Revit. Thus, 3D reconstruction models with complex  
175 architectural shapes are automatically generated as well as through NURBS surfaces. Yet, the  
176 use of several software packages limits the work of BIM operators. The true nature of accurate  
177 3D reconstruction is to automate processes by reducing the number of software applications  
178 used. This is the knowledge gap of 3D Accuracy Reconstruction Geometry (3D ARG).

179 **Semantic segmentation**

180 Reverse engineering is the process of capturing massive data from LiDAR technology.  
181 Therefore, it is an accurate representation of the building shell and its superficial elements.  
182 These data are recorded in files with a large amount of information that are not operational on  
183 a BIM platform. The 3D point cloud shapes fundamental parameters capable of representing  
184 both geometrical components and radiometric elements [29]. Due to the large amount of  
185 information they provide, there are numerous research studies on the subject. One important  
186 area is segmentation algorithms for automatic classification [5,27,28,36,45,46]. Recently, a  
187 large-scale open platform for point cloud processing has emerged. The Point Cloud Library  
188 (PCL) framework contains numerous state-of-the-art algorithms for filtering, surface  
189 reconstruction, model fitting, registration, and segmentation, among others [47]. A review of  
190 these algorithms was carried out by Grilli et al. Hence, for this research, those for model fitting  
191 are the most interesting algorithms. In the field of image analysis and processing, the concept  
192 of semantic segmentation aims to classify each pixel of a scene image. Each pixel is then  
193 allocated to a group in an image, resulting in homogeneous clusters [48]. The most widespread  
194 use of this technique is in the fields of autonomous vehicles, robotics, and indoor positioning  
195 systems [5]. This classification is possible thanks to automatic processes based on Machine  
196 Learning (ML). This technology applies inferences to a given piece of information to  
197 appropriately represent relevant aspects. Thus, segmentation studies are crucial for planning  
198 sustainability strategies and on perception criteria [49]. Segmentation uses ML or Deep  
199 Learning (DL) techniques; their difference lies in the types of algorithms they implement. ML  
200 uses mathematical algorithms, whereas DL is based on biological neural networks of the  
201 human brain [50]. Segmentation within the digital documentation of CH uses these learning  
202 techniques to identify objects. The novelty is the combination of these techniques to work  
203 with point clouds. Here, the method represents considerable benefits in shape detection for  
204 further modelling in heritage environments. The feature classification can be conducted via  
205 pre-training, but also through pre-set training and the interactive method, where complex  
206 mathematical procedures [29] are required to achieve appropriate results. Even so, the use of  
207 these technologies in the three-dimensional domain is rather limited. Some studies used these  
208 methodologies on historical facades to apply 2D to 3D information transfer [51], while other  
209 methods performed semantic point cloud segmentation [5]. These can be conducted by  
210 creating a set of images through the point cloud (Multi-view based), point cloud rasterisation  
211 based on voxels, or by applying a feature-based approach to the points.

212 Other methods related to the above exist in the scientific literature. There are methodologies  
213 involving training from an original (zero) position with previous training of readjustment or  
214 hyperparameter optimisation (impulse, weight drop, or learning rate) [50]. On the other hand,  
215 there are some studies on artificial neural networks (ANN) that can recognise objects, such as  
216 3D ShapeNets [52], or PointNet [53]. Other studies focus on obtaining vector values from  
217 photographs. The classification is performed through three parameters using freely available  
218 software such as AutoTrace, Potrace, or Inkscape. The process consists of interpreting a  
219 bitmap in black and white to produce vectorised curves [54]. For an in-depth analysis of a  
220 polygonal model, other studies simplify complex 3D geometry into a series of 2D closed  
221 polygons by automatically converting each polygonal section into a raster model. All raster  
222 sections produce a 3D volumetric model in a voxel format. This process is called voxelisation  
223 [55][56]. Here, the voxel is to 3D what the pixel is to 2D, i.e. the voxel is the minimum unit to  
224 form a volume. A series of voxels, endowed with information such as position, colour, and  
225 density, allow the generation of a hypothetical 3D model [57]. This methodology intends to

226 reduce the file size, thus reducing the work time as the computations would be much faster  
 227 [58]. In addition to its use in visualisation tests such as x-ray imaging or MRIs, this method is  
 228 also used to detect 3D objects in robotics and autonomous driving [59]. Given that this  
 229 approach is used when high accuracy is required, it could be beneficial for virtual heritage  
 230 recovery. One of the most interesting options for CH modelling could be working with point  
 231 clouds directly without creating meshes. In this sense, it is proposed to use this methodology  
 232 to automatically convert the point cloud into parametric objects, although it would still be  
 233 necessary for the user to operate the programme [56].

234 **Methodology**

235 *1.- Case study*

236 The façade of the Casa de Pilatos, a 16th-century Palace located in the centre of Seville (Spain),  
 237 was chosen as a case study for semantic segmentation. The façade composition is based on  
 238 planes and decorative elements of different architectural styles and with different shapes.  
 239 Thus, the case study is a suitable environment for 3D point cloud data segmentation.

240 *2.- Data acquisition*

241 Image-based methods and 3D laser scanning are the most widely used professional and  
 242 scientific data acquisition techniques for large-scale projects. Of these two techniques, TLS is  
 243 currently the most extensively used, as it provides accuracy and speed. Notwithstanding, other  
 244 researchers have used image-based methods for 3D reconstruction because of their economic  
 245 advantages, efficiency [60], and to ensure fidelity in CH BIM [21,61]. LiDAR technology is based  
 246 on the calculation of the distance between the laser and the object. This procedure is  
 247 developed using the time-of-flight method or through the transmitted and received signal  
 248 waveform [18]. The method performs a scan of the entire surface to capture thousands of  
 249 points in an x, y, z coordinate system to produce the range cloud. In this case study, a Leica  
 250 Geosystems BLK360 laser scanner is used to capture the geometry of the main façade of the  
 251 Palace. This device uses the Waveform Digitising (WFD) technology and has four built-in  
 252 cameras: 3 digital HDR, colour sensor and fixed focal length cameras ( 2592 x 1944 pixels  
 253 resolution, 60° x 45° (V x H), a full dome of 30 images, automatic spatial rectification, 150 Mpx,  
 254 360° x 300°); and an infrared camera (160 x 120 pixels resolution, 71° x 56° (V x H), a full dome  
 255 of 10 images, 360° x 70°). Although the equipment can be controlled using a computer or a  
 256 tablet, the data capture was automatically performed and further processed in the laboratory.  
 257 Additional specifications of the scanner are shown in Table 1.

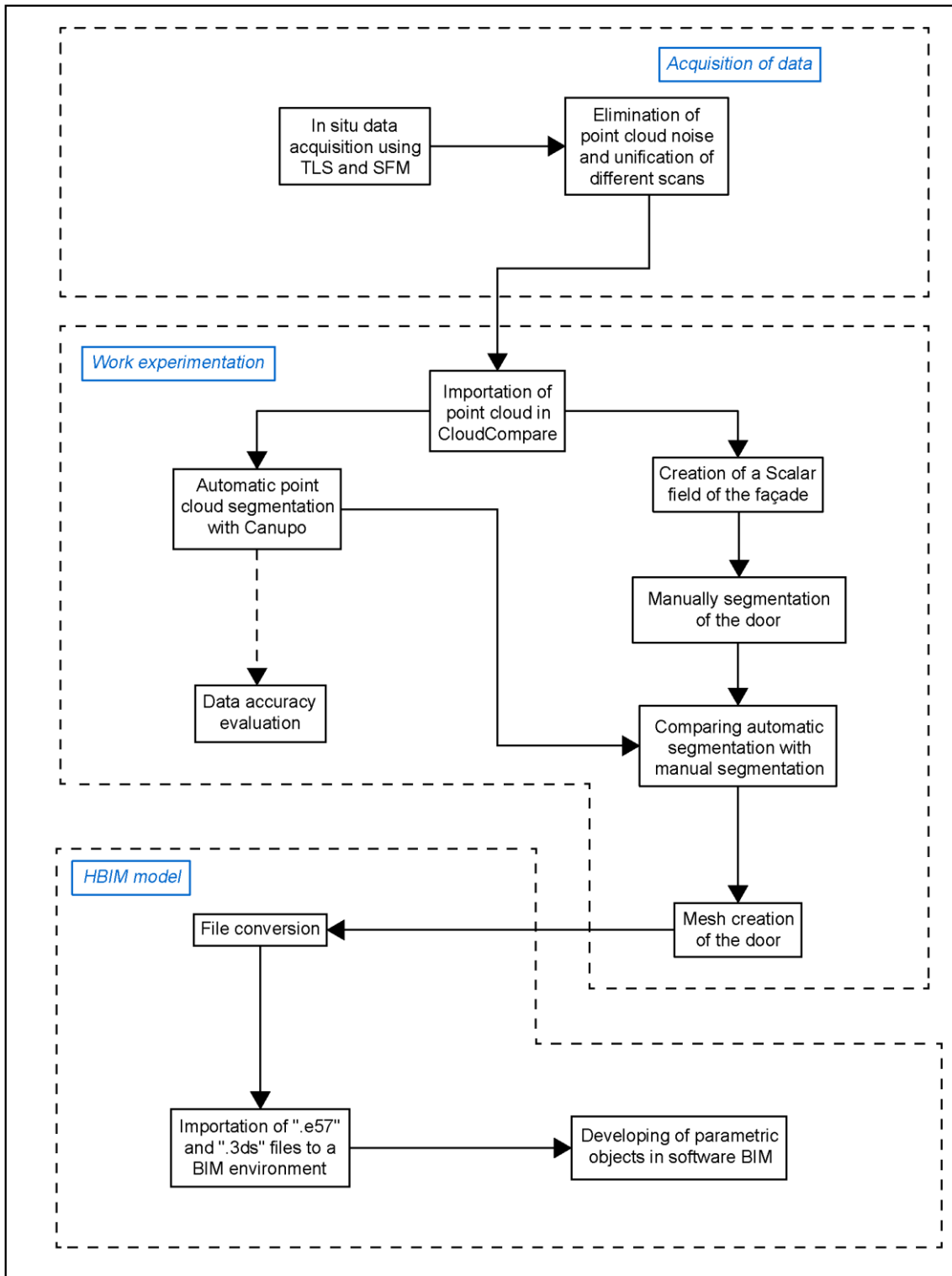
258 **Table 1.** Laser scanner specifications

259

LEICA BLK 360	
Wavelength	830 nm
Field of view	360° (horizontal)/300° (vertical)
Range	Min. 0,6-up to 60 m
Point measurement rate	Up to 360000 pts/sec
Ranging accuracy	4mm @ 10 m/7 m @ 20m
3D point accuracy	6mm @ 10 m/8 m @ 20m

260

261 Figure 1 depicts the research workflow:



262

263 **Figure 1.** Workflow.

264 3.- Post-processing

265 Point cloud processing involves interpreting the spatial components (x,y,z). The segmentation  
 266 and classification of the object are necessary for 3D modelling and the analysis process in the  
 267 research into historic buildings. To prepare the dataset, a filtering of the elements outside the  
 268 range of the main façade is carried out on the TLS global cloud. Points containing residual  
 269 values and outliers are removed using the Leica Cyclone 9.2.1 software (Leica Geosystems,



270 2018). In the segmentation process, the homogeneity criterion is not related to the image  
271 radiometry. The classification of the morphology structure component will be the selection  
272 criterion. Therefore, the façade surface is partially taken, considering its composition based on  
273 planes and decorative components. The point cloud, with 38 million points, is obtained and  
274 transferred to CloudCompare v2.10.2 (Zephyrus) software (Girardeau-Montaut, 2003) for  
275 further processing. From the C2C process, two point subsets are obtained from the façade: a  
276 manually segmented group of elements and the global range cloud. In the 3D point cloud  
277 classification, three types of discrepancies must be taken into account, such as i) the gaps in  
278 the cloud due to laser beam occlusions, ii) the effects that may be caused by shadows on the  
279 scanned elements, and iii) those figures in movement through the architectural spaces.

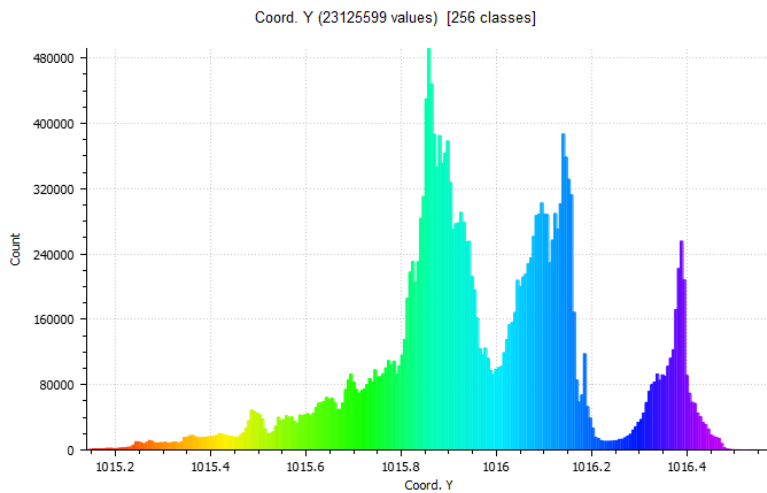
#### 280 4.- Evaluation of the experimental design

281 The 3D object reconstruction is an important step in digital representation since it allows for  
282 approaching the physical world as a basis for analysis and construction [31]. Modelling has  
283 therefore been considered as a digital representation comprising simplified geometric  
284 properties of heritage buildings. In this sense, models represent the three dimensions of space  
285 in real time, but it is the BIM platforms that include semantic components, represented as  
286 digital objects comprising relationships, attributes and properties[62]. These objects in historic  
287 buildings generally have complex geometric elements, as in the case of natural shapes such as  
288 trees, rocks, and grass. This paper hypothesises that Brodu and Lague's algorithm [7], which  
289 was developed for these complex terrain geometries, should apply to the morphology of  
290 heritage buildings. Also, to the best of our knowledge, this algorithm has not been applied to  
291 heritage elements before. This algorithm is effective in the classification of natural surfaces  
292 through the local analysis of changes in the geometrical properties of the point cloud. It is  
293 available in CloudCompare software [8] as the CAracté-risation de NUages de POints (CANUPO)  
294 plug-in to work as a 3D multiscale classifier by training elementary binary classifiers. The basic  
295 working principle of this algorithm is to project a sphere with a radius depending on the  
296 working scale onto a point in the scene; next, the geometrical behaviour of neighbouring  
297 points in three dimensions is analysed in this space. Brodu and Lague applied this system to  
298 natural scenes of a subset with a range of scales to recognise rocks, vegetation, water, and  
299 gravel in the Otira riverbed (New Zealand). The procedure relies on the combination of C2C  
300 classifiers, working in two different ways. The first approach executes the "Classify" command,  
301 using the available classifiers created by default. The second method creates customised  
302 "Train Classifier" classifiers. Once the point cloud is obtained, the system performs training  
303 through different parameters: the measurement range, measurement scale, and point  
304 sampling. Yet, the idea behind the classification procedure is the combination of scales, where  
305 dimensionality makes it possible to distinguish from more than one category [7]. The  
306 mathematical rationale was made explicit in section 3.1 Local dimensionality at a given scale.  
307 The tool determines the degree to which a local neighbourhood of points can be considered 1-  
308 D, 2-D or 3-D by finding the components of the coordinates of the points in the neighbourhood  
309 [63]. Local dimensionality analysis for characterising the point cloud at different scales [64] can  
310 be expressed as follows: for 1D, the points belong to a line, in 2D, to a plane surface, and to a  
311 volumetric surface in 3D. Finally, a discriminative analysis is applied to find the hyperplane of  
312 maximum classification separability.

#### 313 4.1.- Manual segmentation through the scalar field

314 The evaluation process is carried out by means of a complementary study and analysis. To this  
315 end, a point set from manual semantic segmentation comprising three testbeds is obtained.

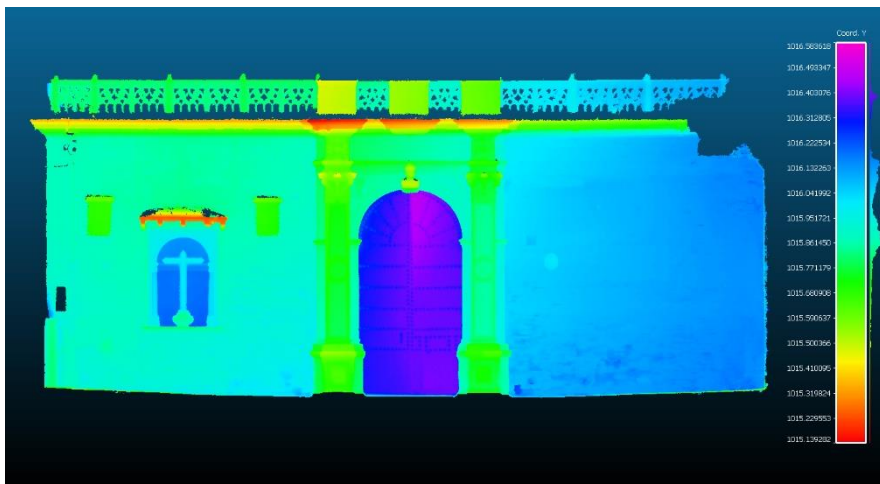
316 This process is common in scientific literature. Kovanič et al. [65] used manual segmentation to  
 317 process point cloud data and determine the geometric parameters of a rotary kiln. Li et al. [66]  
 318 used manual segmentation to automate the analysis of building facades from TLS. The purpose  
 319 was to semantically segment and label the depth planes. Manual refinements are sometimes  
 320 used in point cloud segmentation in tree structure studies [67]. However, manual  
 321 segmentation involves a laborious and time-consuming task. The more complex the scene is,  
 322 the more difficult it is to process [68]. The main challenge is to match the morphology of the  
 323 architectural elements. Likewise, because it is a manual process, the point subsets taken may  
 324 or may not belong to the geometry of the chosen element. Considering the limitations of  
 325 manual segmentation, a scalar field is created to classify the façade's point cloud according to  
 326 values on the "y" axis, as established by the C2C software's coordinate system (Figure 2).



327

328 **Figure 2.** Façade's scalar field.

329 This process involves classifying the points in space with respect to a (x,z) plane. In other  
 330 words, the distances from the point cloud to a theoretical (x,z) plane are being calculated. The  
 331 result of the process is a scalar value for each point in the cloud that indicates the Euclidean  
 332 distance between the analysed point and the closest point to the imaginary plane. The results  
 333 are displayed in the histogram in Figure 3.



334 **Figure 3.** Histogram of the number of points between the reference plane (x,z) and the Y-  
 335 coordinate.

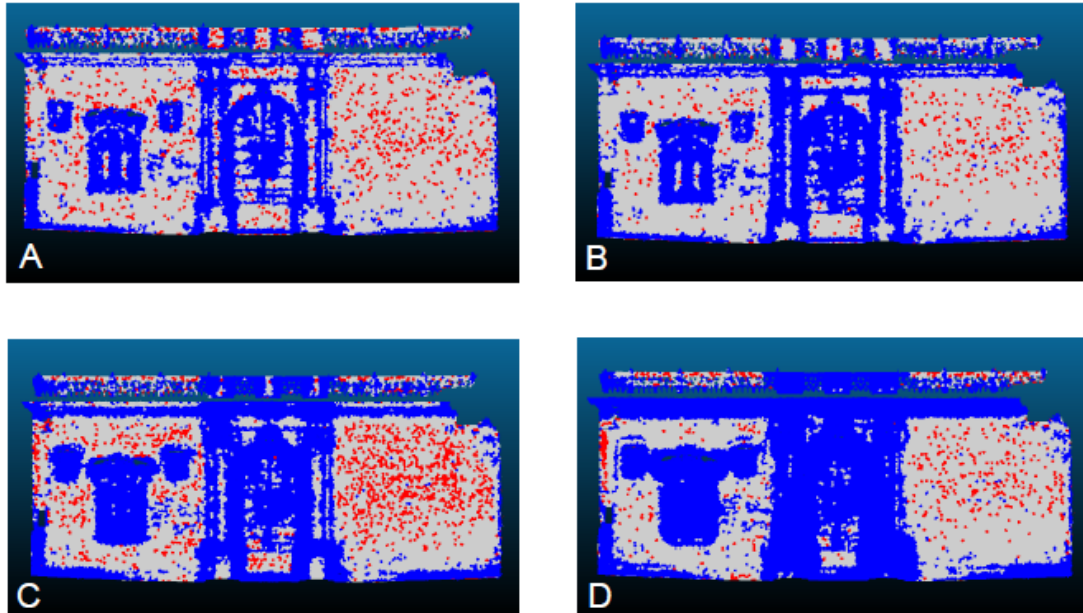
336 It should be noted that manual segmentation may capture points outside the chosen model  
337 since there would not be a segmentation of classification with certain parameters.

#### 338 4.2.- Algorithm validation testbeds

339 In order to test the applicability of the classification algorithm, three testbeds were carried  
340 out. First, working with the global point set, i.e. considering the complete façade (21.00 metres  
341 long by 8.50 metres high (Figure 4)), the parameters were adjusted according to the length of  
342 each element.

343 Marble shapes were initially differentiated from the predominant brickwork: the three  
344 parameters involved in the process were minimum distance, interval, and maximum distance.  
345 The minimum distance is the smallest magnitude between the elements to differentiate. For  
346 example, the length of a brick or a rivet in wooden doors, among others. The maximum  
347 distance is the opposite, the largest dimension of the elements. In this case, the height of the  
348 pilasters that form the centre of the marble doorway was considered. Finally, the intervals to  
349 determine the total number of scales needed were chosen.

350



351

352 **Figure 4.** (a) Test A; (b) Test B; (c) Test C; (d) Test D. Classification through the CANUPO  
353 plug-in. The red dots represent the bricks and the blue dots represent other materials.

354 The images show the point density of a scene represented in the proposed feature space at  
355 different scales. Each image represents the working process with the C2C tool to measure the  
356 distances for the chosen architectural elements. Meanwhile, the larger the maximum distance,  
357 the longer the processing time. Similarly, the smaller the interval, the longer the processing  
358 time. In the analysis, tests were conducted by choosing alternative measurements according to  
359 Table 2.

360

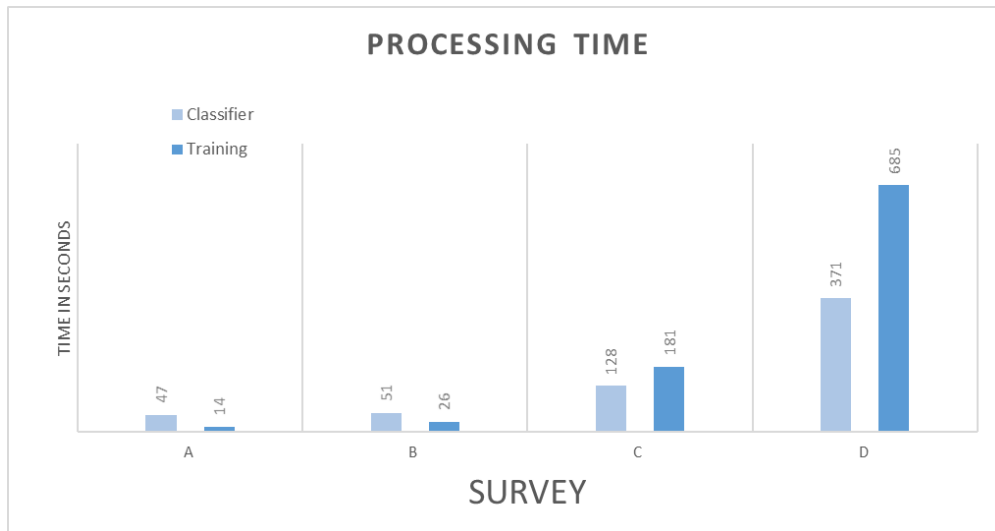
**Table 2.** Distance parameters taken for global façade processing

361

	Min. Distance (m)	Step (m)	Max. Distance (m)
Survey A	0.01	0.025	0.50
Survey B	0.01	0.01	0.50
Survey C	0.01	0.01	1.00
Survey D	0.01	0.01	1.50

362

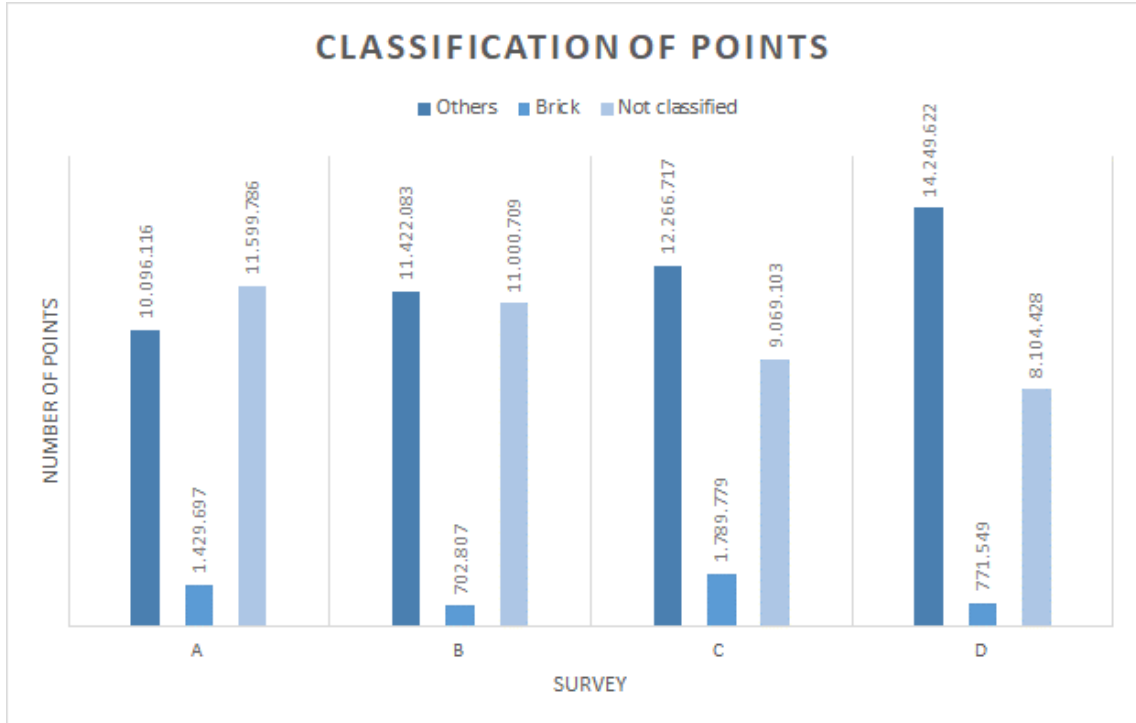
363 Also, various graphs were produced to evaluate the data obtained and to verify the software  
364 performance. Comparisons were carried out of the tests in which the processing time, the  
365 number of classified points, and the precision of each sample of the sets were represented. It  
366 should be noted that the processing time depended on the hardware used, a computer of  
367 average specifications (Intel i5 processor with 12 GB RAM). Each step was measured (Figure 5).  
368 The number of classified points represents the subsets that can later be used to generate  
369 meshes for conversion into parametric BIM objects. The accuracy is a magnitude achieved  
370 through the experimental values entered into the software. For example, for this case,  
371 measurement distances of 10 cm were taken.



372

373 **Figure 5.** Processing time for each test A, B, C, and D of the training and classification  
374 using the CANUPO algorithm.

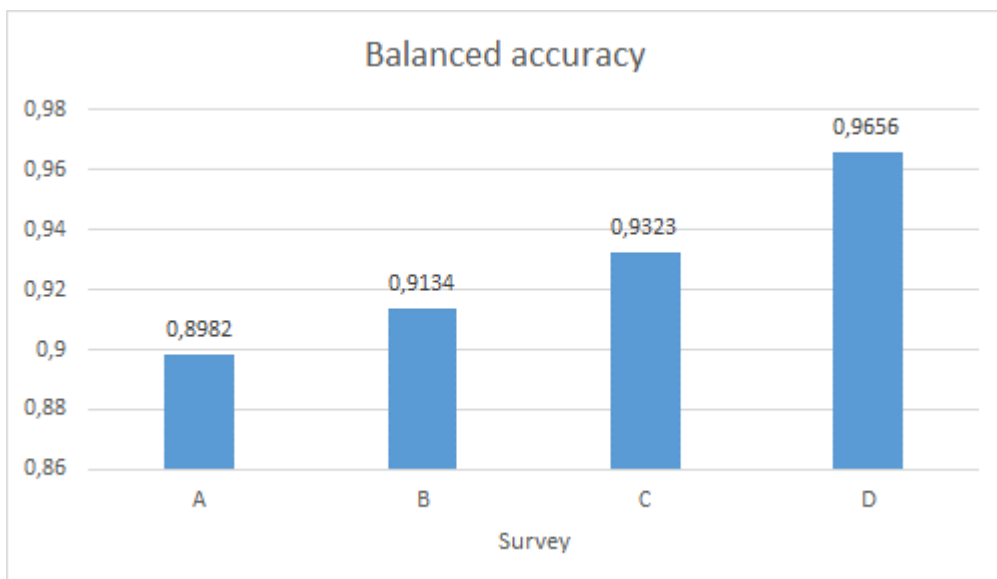
375 Following the classification procedure, the best combination of selection scales was defined.  
 376 The operator can then determine the scale range of the different categories and elements to  
 377 be geometrically classified. According to Brodu and Lague, the algorithm finds the best  
 378 combination of scales to segment into different categories previously defined by the operator,  
 379 as shown in Figure 6.



380

381 **Figure 6.** Point classification in the global façade. Tests A, B, C, and D.

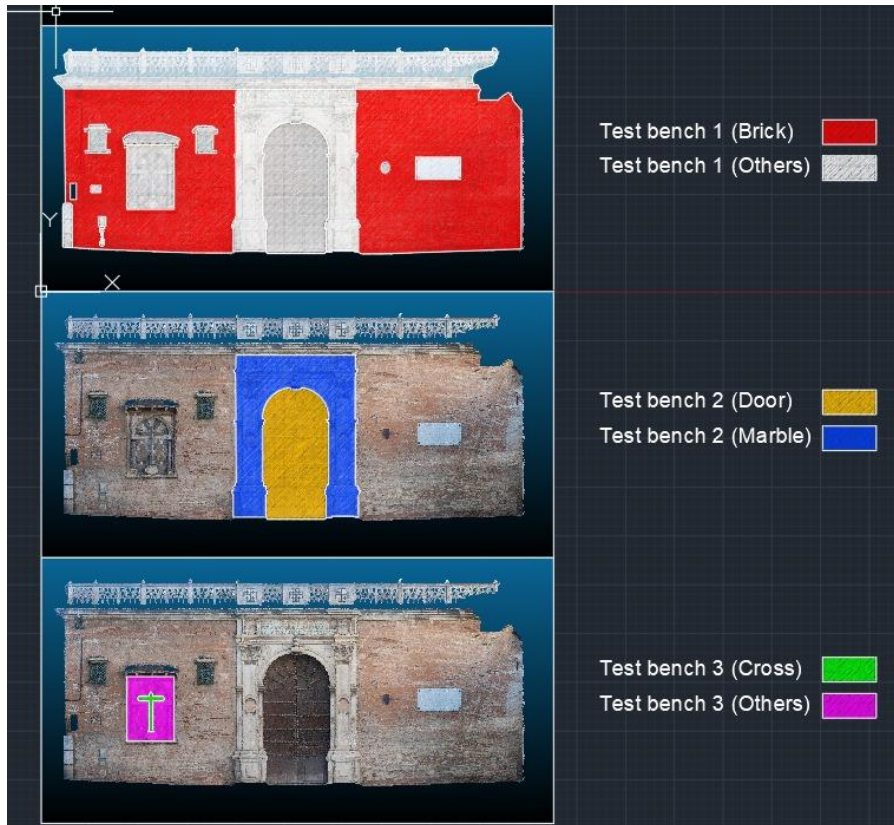
382 Figure 7 shows the Balanced Accuracy (BAa) value. With this value and that of the FDRfdr  
 383 (Fisher Discriminant Ratio), the performance can be measured by classifying each point in its  
 384 respective class. This data appears as a supplement in the statistics section once the first  
 385 phase, the training, is carried out. The result of this phase is a .prm file.



386 **Figure 7.** The accuracy achieved in tests A, B, C, and D. Sampling over 10,000 points of  
387 survey items.

388 Each test was analysed to determine the classification percentage of points in the façade  
389 global point cloud. 49.84% was obtained for survey A, 52.43% for survey B, 60.78% for survey  
390 C, and 64.95% was achieved for survey D.

391



392

393 **Figure 8.** The schemes of the three testbeds.

394 The second testbed addresses the main entrance to the Palace, focusing on the area delimited  
395 by the two pilasters and the lintel of the portico (3.50 metres wide by 7.55 metres high). The  
396 hardwood door is selected, the marble pilasters are differentiated, and the brickwork is  
397 omitted (Figure 9).

398



399

400 **Figure 9. (a) Test E; (b) Test F. Classification through the CANUPO plug-in.**

401

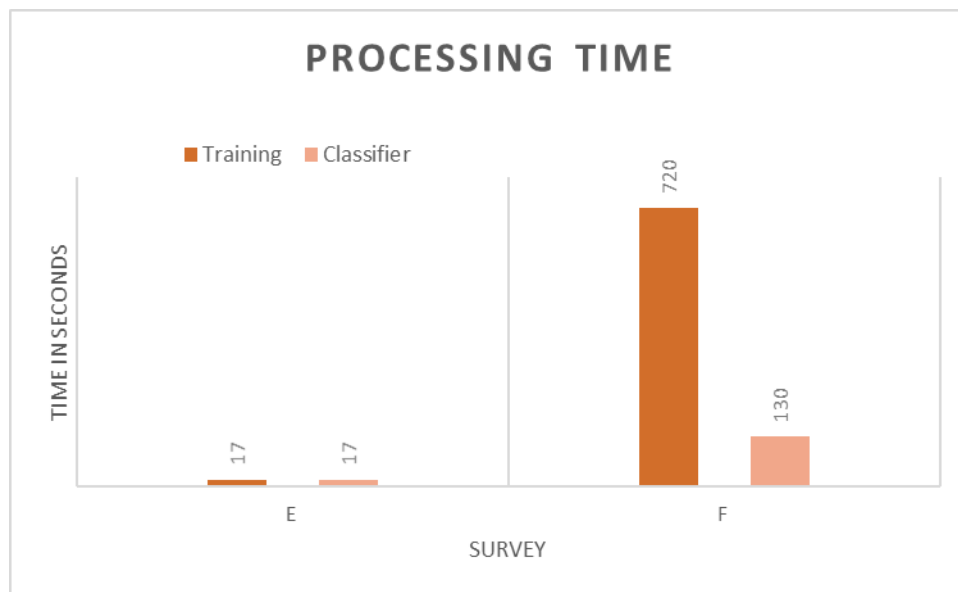
402 **Table 3.** Distances taken to process the façade portico.

403

	Min. Distance (m)	Step (m)	Max. Distance (m)
Survey E	0.01	0.025	0.50
Survey F	0.01	0.01	1.50

404

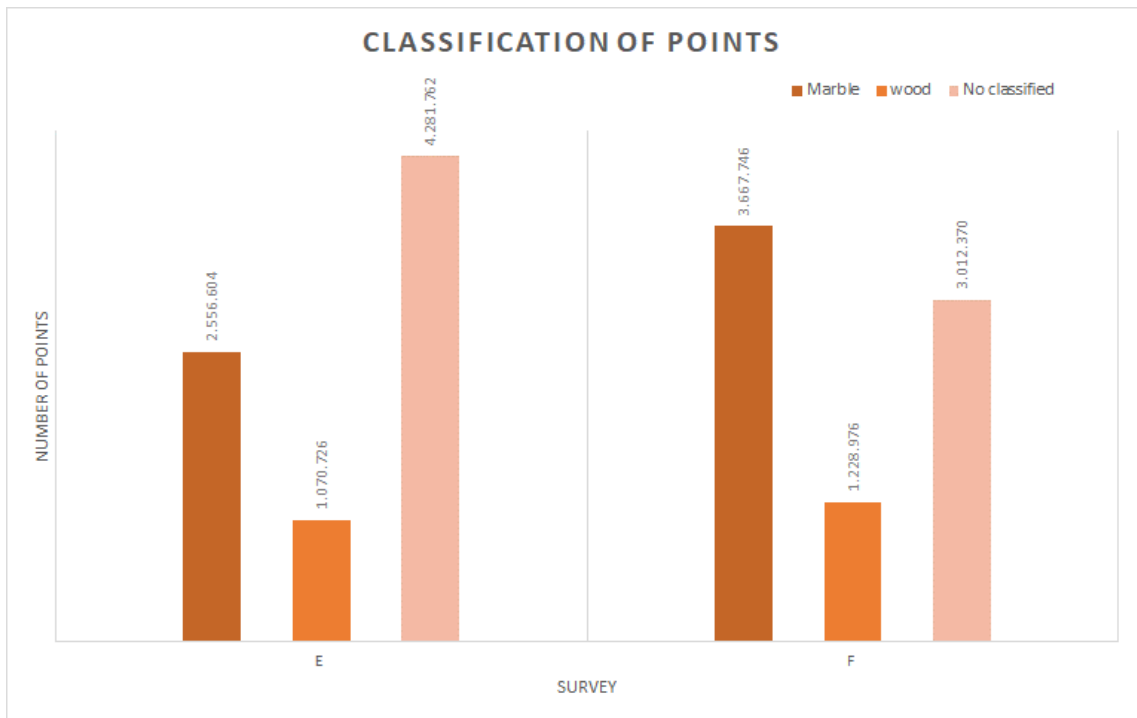
405 The same procedure enabled comparisons of the tests by plotting the accuracy obtained, the  
406 processing time, and the number of classified points for each data set sample.



407

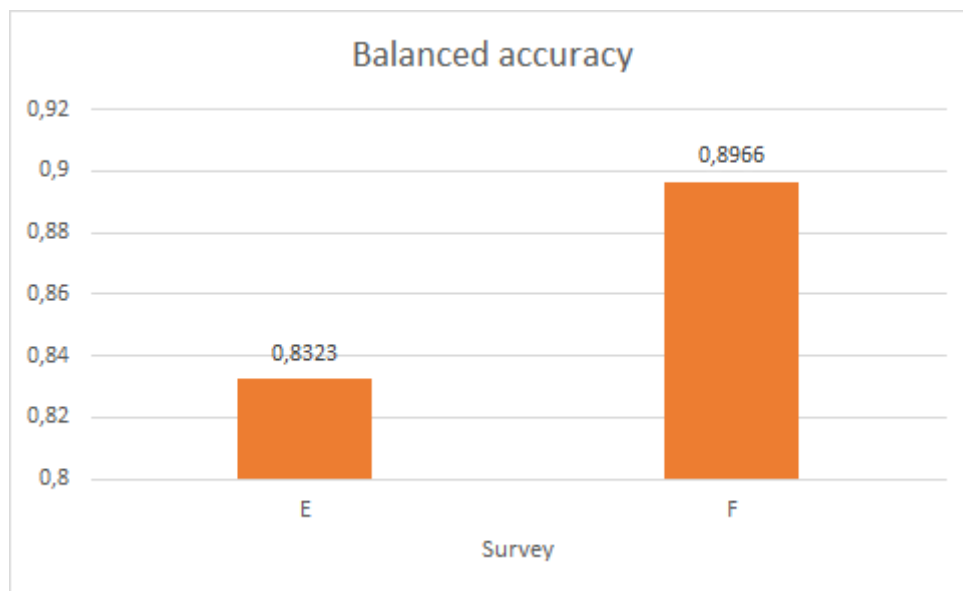
408  
409

**Figure 10.** Processing time for the training and classification tests E and F using the CANUPO algorithm.



410  
411

**Figure 11.** Point classification of the façade portico in tests E and F.



412  
413  
414

**Figure 12.** The accuracy achieved in tests E and F of the marble portico and the wooden door. Sampling over 10,000 points of study elements.

415 Regarding the percentages of points classified in the façade portico corresponding to the two  
416 materials analysed, the marble of the entrance portico and the wooden door, 45.86% was  
417 obtained in survey E and 61.91% in survey F.



418 For the third testbed, the retablo on the left side of the façade was chosen. It is a piece carved  
 419 in different marbles in various shades of colour. The dimensions of the chosen area are 1.75  
 420 metres wide by 2.35 metres high, as in the marble frame. It has been chosen for its  
 421 morphological singularity, a miniature retablo composed of two columns on a round arch and a  
 422 Christian cross in the centre (Figure 13).



423 **Figure 13.** Processing time for training and classification tests E and F using the  
 424 CANUPO algorithm.



425  
 426 **Figure 14.** (a) Test G; (b) Test H. Classification through the CANUPO plug-in.

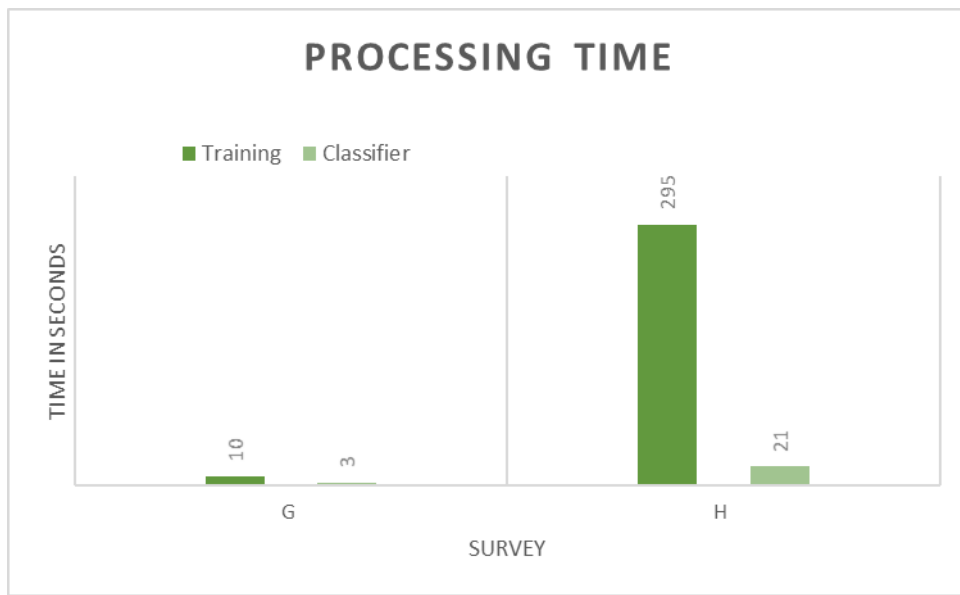
427 The results of tests G and H are shown in graphs according to the accuracy achieved, the  
 428 processing time, and the number of classified points of each data set sample. The distances  
 429 taken for the processing of the retablo are shown in Table 4.

430 **Table 4.** Distances taken to process the retablo.

	Min. Distance (m)	Step (m)	Max. Distance (m)
Survey G	0.01	0.025	0.50
Survey H	0.01	0.01	1.50

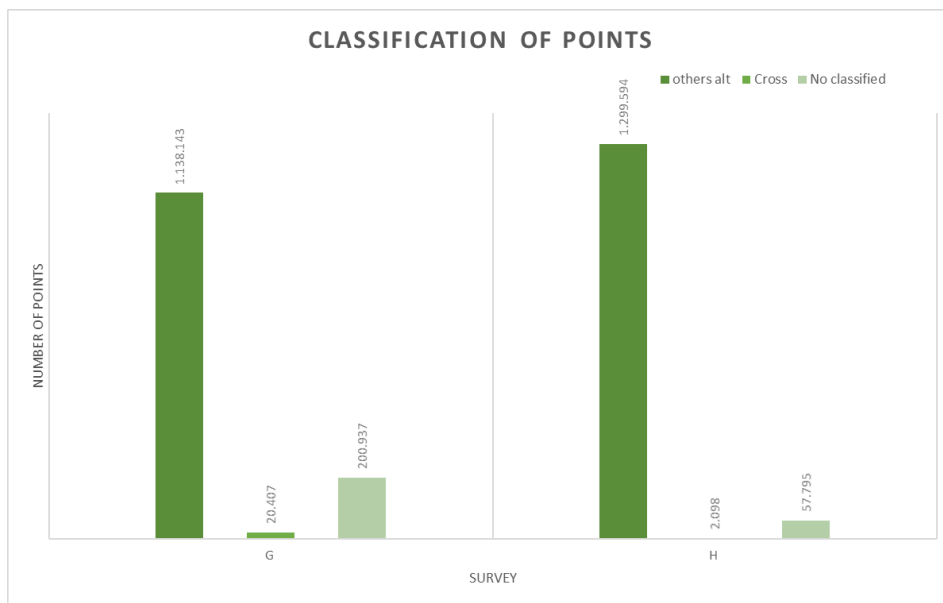
432

433 Next, comparative tests were carried out, and the processing time is shown in Figure 15.



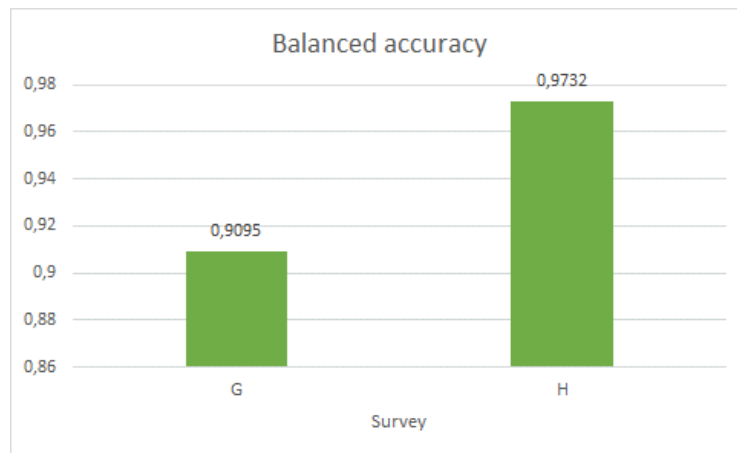
434

435 **Figure 15.** Processing time for training and classification tests E and F through the CANUPO  
436 algorithm.



437

438 **Figure 16.** Point classification on the façade portico in Tests G and H.



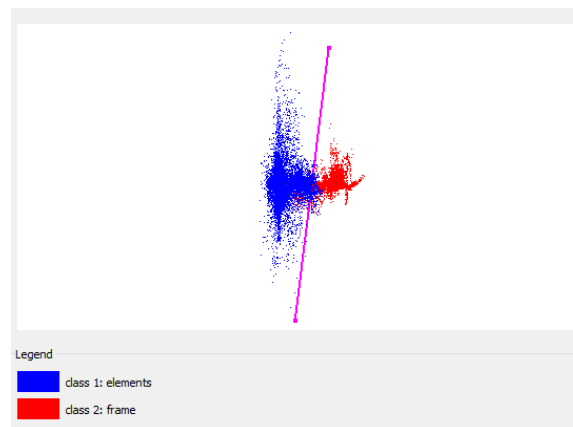
439

440 **Figure 17.** The accuracy achieved in tests G and H. Sampling over 10,000 points of  
441 survey items

442

443 The point classification percentage in the retable (different types of marble in various colours)  
444 was also determined. 85.22% was achieved in test G, and 95.75% in test H.

445 CloudCompare software using the CANUPO algorithm allows the operator to obtain a  
446 probabilistic classifier. This classifier firstly defines the projection of the data onto a plane of  
447 maximum separability to, secondly, separate the classes. The main advantage of this is that an  
448 immediate and intuitive visualisation of the classification process (Figure 18) is obtained. The  
449 reliability level is set on the abscissa axis and the ordinate axis sets the range.

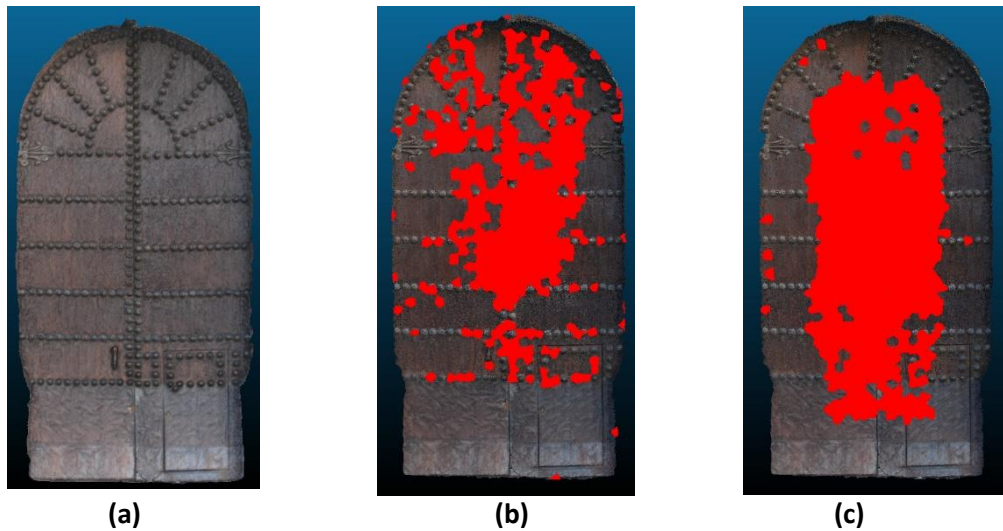


450

451 **Figure 18.** Classifier definition in the plane of separability.

452 Once the manual segmentation through the scalar field and the point classification process  
453 with the CANUPO algorithm have been carried out, the modelling of the gate was undertaken  
454 (tests E and F). The gate was segmented according to Figure 19. For the manual semantic  
455 segmentation of the point set and its segmentation using the CANUPO algorithm, a reference  
456 was established in percentages of the number of points captured; next, the creation of the  
457 BIM took place. In this case, the manual segmentation was taken as a reference, with which

458 2,535 points were obtained. Figure 19a shows (red colour) the projection of the point set  
459 selected by the algorithm in tests E and F compared to the total number of manually  
460 segmented points of the gate.



461

(a)

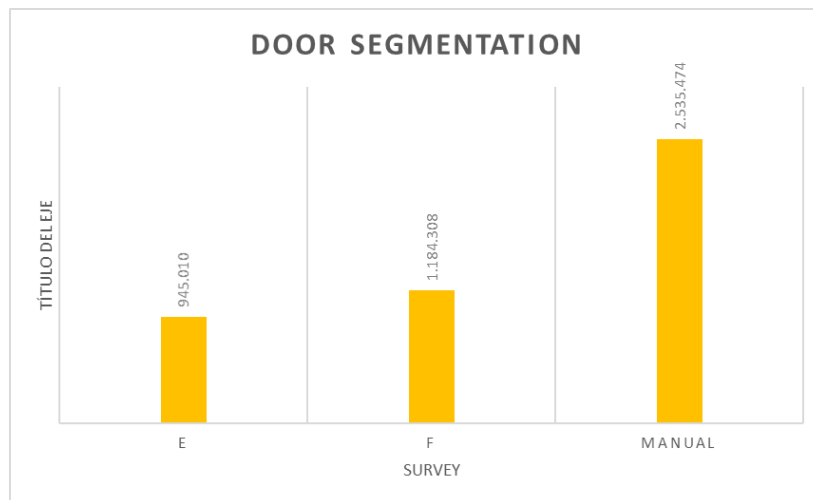
(b)

(c)

462 **Figure 19.** (a) Manually segmented point set, (b) test E, and (c) test F.

463 The point set taken as a reference was considered 100% of the points (Figure 19 a). 37.27% of  
464 the manually segmented points were classified in test E, and 46.71% in test F. Figure 20 shows  
465 the number of points of each test.

466



467

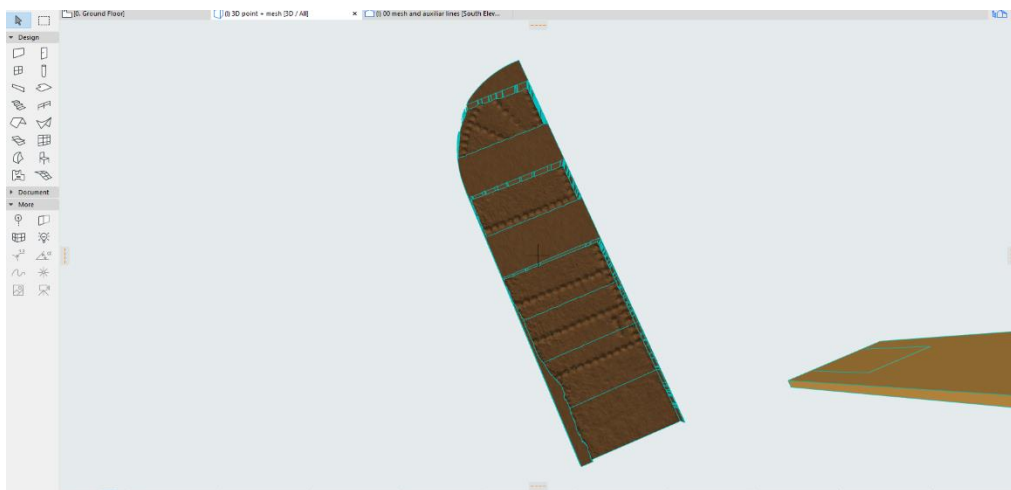
468 **Figure 20.** The number of points obtained from segmentation tests E and F against manual  
469 segmentation (M).

#### 470 5.- Modelling the tests in BIM

471 An important factor in the parameterisation process is determining the geometry. The process  
472 of transferring TLS or SfM to BIM is known as Scan-to-BIM [69]. The Scan-to-BIM framework is  
473 specifically designed to ensure that BIM meets the applicability requirements for CH, whether  
474 architectural or archaeological, by efficiently managing the information provided by data  
475 capture techniques. Wang et al. [70] determined four fundamental steps in the process,

476 including the identification of information requirements, scan data quality, data acquisition,  
477 and BIM reconstruction. This involves creating the BIM with the geometric parameters  
478 provided by the MDCSs. In practice, the MDCS files are imported into the BIM tools and serve  
479 as a reference template for modelling. Nevertheless, this procedure can be prone to errors. To  
480 overcome these issues, previous research has addressed the semi-automatic generation of  
481 parametric objects from TLS or SfM point clouds. Antón et al [40] evaluated the accuracy of  
482 the 3D meshing from remote sensing products to later propose a semi-automatic three-stage  
483 procedure to create an as-built HBIM. For their part, Andriasyan et al [39] explored the  
484 combination of Rhino+Grasshopper-ArchiCAD software to automate the Scan-to-BIM process.  
485 In this paper, effective procedures to automatically build parametric objects are explored,  
486 which is a knowledge gap in the field. To validate the data obtained (the points segmented  
487 using the CANUPO plug-in), the workflow by Moyano et al. [71] for complex surfaces common  
488 in architecture and archaeology is used.

489 Surveys M (Manual), E, and F were exported to Rhinoceros in .ASCII or .e57 formats for their  
490 conversion into meshes, in the same way as the subset obtained by segmentation through the  
491 scalar field. The meshes were inserted into the BIM software (ArchiCAD) to be transformed  
492 into .gsm parametric objects, in such a way that the actual geometry of the wooden door was  
493 generated. However, the meshes can also be subsequently transformed into 'Morph' elements  
494 for editing and customisation in the HBIM project. In this case, the Boolean operations  
495 between elements was the procedure chosen. To define the surface faces of the door with a  
496 thickness of 8 centimetres, division surfaces were used, thus performing a subtraction with  
497 extrusion upwards as an operation between solid elements in the BIM platform. This  
498 procedure was carried out for both faces to achieve a model as shown in Figure 21. The model  
499 used the manually segmented TLS point cloud, as it was the most complete of all surveys. This  
500 procedure verified the Scan-to-BIM methodology for the system requirements. Hence, the  
501 parametric modelling was validated for the case of the manually segmented point set from the  
502 scalar field of the main façade.



503 **Figure 21.** Relief of the wooden door solid object.

504

### 505 5.1 Modelling results

506 3D modelling has been particularly conducted for civil engineering applications and games  
507 based on real-world environments [72]. With a view to approximate real shapes, BIM

508 technology has implemented processes to manually and automatically create geometric  
509 models from point cloud data. The point cloud representing complex architectural shapes can  
510 be translated into triangulated meshes before generating the parametric objects. This is a  
511 common workflow established by specialists in the field, a further stage involved in the Scan-  
512 to-BIM to the Mesh-to-BIM process. That transformation requires using different programmes.  
513 Yang et al. [73] followed a three-step process: the extraction of basic primitives in 3D in  
514 Rhinoceros software, the transformation of surfaces to volumetric components using extrusion  
515 and NURBS functions in the same programme, and the generation of Dynamo visual  
516 programming algorithm packages. This process is rather complex and would require that the  
517 BIM operators specialise in various software. In this paper, the whole process was carried out  
518 using Rhinoceros and ArchiCAD. The result of the tests is shown in Figure 22.

519



520

521 **Figure 22.** Global point cloud of the façade and BIM of the door.

522

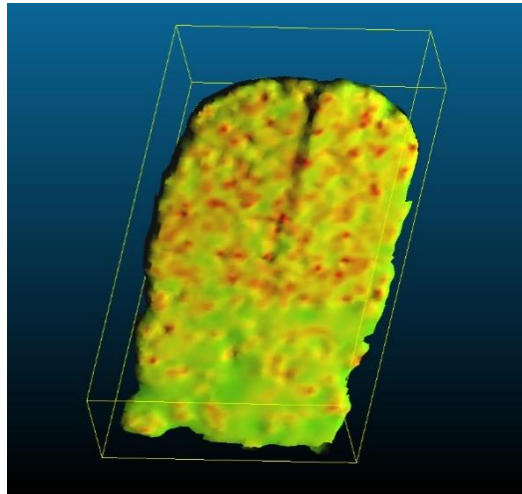
### 523 *5.2.- Point cloud decimation validation within the Mesh-to-BIM process*

524 To validate the expected point density of a parametric model, the point set of the manually  
525 segmented wooden door was decimated. The data were next taken to the C2C software to  
526 reach the desired resolution. Optimal values of the segmentation parameters were also sought  
527 so that the smallest number of points would provide representative data for the Mesh-to-BIM  
528 process. Test work was carried out starting from 100 points per square metre to know the  
529 scope of the work. This point density was initially established by Pu and Vosselman [30] for  
530 their experimental work on an automatic method for the reconstruction of building façades. In  
531 this paper, the data consist of a point subset of 2,535 points. Using the subsample command  
532 with random parameters, a decimated subset of 2,000 points was obtained, which entailed  
533 approximately 110 points per square metre (Figure 23). In the second phase, further  
534 decimation of 10,000 points spread over the entire surface of the wooden door was carried  
535 out, resulting in approximately 600 points per square metre (Figure 24). Afterwards, the Mesh-  
536 to-BIM process was performed using Surface Poisson Reconstruction [74].

537 As a result, through a scalar function adjustment, a bubble was obtained by connecting all the  
538 related points. By reducing the density in the SF display parameters, part of the bubble was

539 removed. The decimation results are shown in Figures 23 and 24, and the histograms of the  
540 achieved point densities are presented in Figure 25.

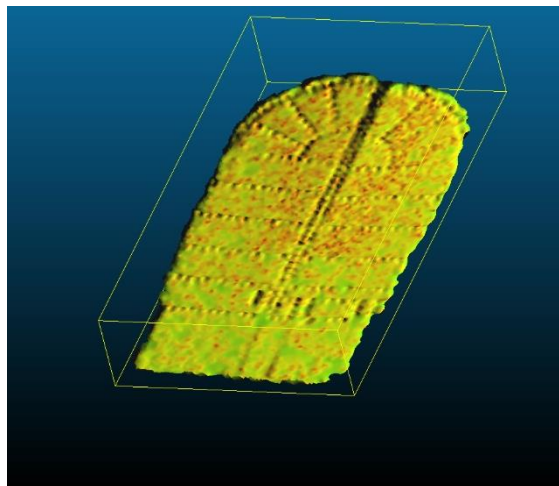
541



542

543 **Figure 23.** Mesh reconstruction of the survey M point set at 110 points/m2 density.

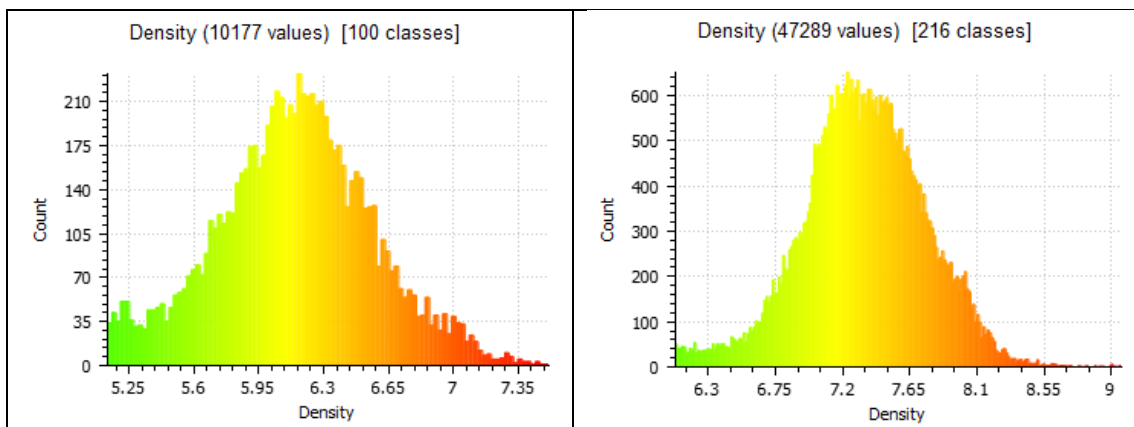
544



545

546 **Figure 24.** Mesh reconstruction of the survey M point set at 600 points/m2 density.

547



548 **Figure 25** a) Histogram of the survey M point set at 110 points/m<sup>2</sup> density. b) Histogram of the  
549 survey M point set at 600 points/m<sup>2</sup> density.

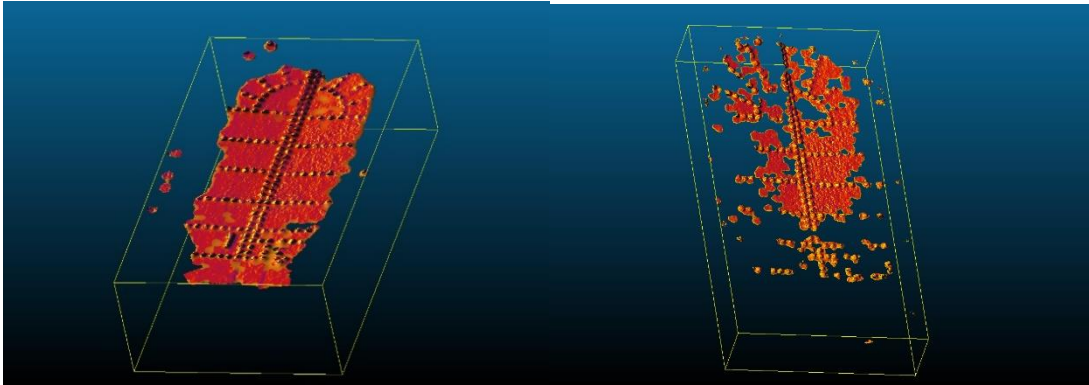
## 550 **Discussion of results**

551 Most studies on semantic segmentation use programming algorithms beyond the software  
552 available to BIM operators. This work advances upon the applicability of the CANUPO  
553 software, which is a plug-in to C2C, well known within the scientific community. This algorithm  
554 was tested to verify that semantic segmentation can provide a representative sample point set  
555 to mesh and subsequently build parametric BIM objects. To do this, point cloud data from  
556 elements analysed within the façade of the 16th-century Casa de Pilatos Palace in Seville,  
557 Spain, were considered. Brodu and Lague's natural surface classification algorithm cannot  
558 detect the presence of changing materials on the same surface but works by the degree of  
559 geometric heterogeneity, where a single scale can rarely classify a scene [7]. To test its  
560 applicability to CH, the aforementioned façade was taken, which presents several complex  
561 geometries of different architectural styles, thus being a suitable example for experimentation.  
562 Three testbeds were carried out; first, the architectural elements comprising the entire façade;  
563 second, on the main gate; and third, on a small retable located on the left side of the façade  
564 canvas. Results on the first testbed show that the classification is less dispersed (test A) by  
565 considering low values (Table 2). In test D, the accuracy increases, as does the number of  
566 unclassified points. The accuracy determines the number of points the algorithm can detect.  
567 This could indicate that points may not be properly classified. To achieve an adequate  
568 classification of the points, it was considered that the representativeness should be at least 75  
569 % of the global set and sufficiently sparse for Mesh-to-BIM. The classification must be based  
570 on a previous decimation of the point subsets (section 4 of this paper). In the second testbed,  
571 test F shows a higher accuracy and marble and wood are above the unclassified ones. The  
572 higher the accuracy, the more significant the points of the wooden door are. In the last testbed  
573 (retable), the classification did not distinguish between architectural elements. Here, the  
574 automatic segmentation process presented serious difficulties for comprehensive modelling as  
575 in Figure 18. Therefore, the exact control of the geometry of the wooden entrance door is  
576 questionable. In view of the results, the CANUPO classification algorithm is more successful on  
577 large complex façades than on minor details such as the small marble retable. In this case, the  
578 algorithm fails to classify the elements of the cross concerning the planes and elements of the  
579 cornice. The tested scale yields a better classification when the base exceeds 10 metres in  
580 length.

581 Another interesting parameter is the time the algorithm takes to classify the selected point  
582 sets. This variable is of interest to the BIM operator, as it influences the operational  
583 performance of the process. Generally speaking, the processing time in tests A, B and C for  
584 both classification and training was a few minutes. Meanwhile, in test D, where the maximum  
585 training distance was taken, the time was approximately 12 minutes and 6 minutes for  
586 classification. In this case, the percentages of classified points were even lower than 70 %. For  
587 the second testbed, the results could be improved, since the processing time was 14 minutes  
588 for 61.91% of classified points. In the third testbed, the processing time was 5 minutes for  
589 95.75% of classified points, although no positive classification results were obtained.  
590 Therefore, a multiscale point cloud analysis was introduced to semantically segment  
591 architectural elements through an open-source algorithm accessible to all researchers,  
592 academics and professionals in the Architecture, Engineering and Construction (AEC) industry.



593 The creation of cross-sections of the wooden door parametric model revealed heterogeneity  
594 of the points and the morphology achieved with respect to the TLS data and the semantic  
595 segmentation model. The results determined the absence of points in important parts in the  
596 point set post-processing for Mesh-to-BIM. The percentage of gaps is due to the partial  
597 segmentation by the classification algorithm, thus losing part of the important elements for  
598 meshing. Part of the classification point sets yielded non-representative data. Figure 26 shows  
599 the results of two tests of the meshing of the wooden door using C2C and the CANUPO  
600 algorithm.



601  
602 **Figure 26.** The meshing of the wooden door in C2C. (a) Test E. (b) Test F.

603 The validation of the point set decimation for Mesh-to-BIM determines that a density of at  
604 least 600 points per square metre in the segmentation is necessary to obtain a representative  
605 sample of the mesh for BIM parameterisation. According to Pu and Vosselman [30], over-  
606 segmentation is preferable to under-segmentation when large elements coexist. In this paper  
607 (section 4.2), a minimum spacing of 6 centimetres is recommended as the optimal value for a  
608 subset of segmented points.

609 Many of the developments and implementations in the specific area of BIM are thanks to the  
610 growing popularity of Open Source Software (OSS) or freeware, which together with Industry  
611 Foundation Classes (IFC) file viewers and exporters allow to reach a large number of users.  
612 [75]. The development of OSS is pursued to permit the enhancement of the collaborative  
613 openBIM® process, as defined by buildingSMART, with the scope of wider “accessibility,  
614 usability, management and sustainability of digital data” [76]. In this case, ArchiCAD can be  
615 operated under an educational licence, while CloudCompare is open source software. The  
616 importing of both point clouds and meshes is implemented in this BIM software. However, the  
617 segmentation through classification elements could lead to a greater operability between  
618 point cloud and digital BIM platforms [77]. In particular, BIM models, with their ontological  
619 structure of elements and semantics, can be widely shared via cloud-based and web-based  
620 platforms. For example, BIMServer [78] is an open source tool to share BIM projects in online  
621 server or local (localhost); or the IFC Web Server [79] consents to visualize the 3D model and  
622 its ontological structure in IFC standard [80]. Nevertheless, architectural heritage visualization  
623 and conservation state analysis require that the real appearance is maintained; for this, open  
624 source web based publisher can be employed for semantic segmented 3D models (point  
625 clouds and meshes), based on WebGL libraries, such as Potree and three.js [81]. In addition,  
626 decimating the point cloud as a simplification approach for BIM as in this research is a practical  
627 resource for streamlining the workflow.

## 628 **Conclusions**

629 In this work, the applicability of Brodu and Lague's algorithm [7] was explored in architectural  
630 elements of heritage sites. Based on the acquisition of TLS data from a façade of the Casa de  
631 Pilatos Palace, an experimental process was developed through three testbeds. A semantic  
632 segmentation method was followed based on open-source software applications such as C2C  
633 that are easy to use by operators, academics and BIM researchers, without the need for  
634 programming. Therefore, the aim was to recognise common morphological features in  
635 heritage buildings, so that complex geometries could be identified.

636 As explained above, the use of these algorithms is sometimes not within the reach of the usual  
637 BIM operators. Firstly, the programmes used generally derive from mathematical work, which  
638 requires a process and knowledge in computational mathematics and visual geometry.  
639 Secondly, not all point cloud data captured by acquisition techniques such as TLS or SfM are  
640 valid. Most segmentation algorithms work with structured or LiDAR files only.

641 Brodu and Lague developed the system on natural scenes of a subset to recognise rocks,  
642 vegetation, water, and gravel in a riverbed. However, this work aimed to experiment with the  
643 geometric fidelity that semantic segmentation can achieve for classifying architectural  
644 elements under CANUPO plug-in training. Given that these tests have not been applied before,  
645 the methodology adopted is original. Also, the validation analysis of the Mesh-to-BIM process  
646 has not been presented before. In order to select the most suitable process to obtain data for  
647 HBIM parameterisation, the results of the algorithm were compared with the manual  
648 segmentation and the selected point set was evaluated. Examining these subsets is essential to  
649 verify their suitability for accurate 3D geometric reconstruction. This paper also discusses an  
650 optimisation framework to analyse other segmentation software to produce parametric BIM  
651 objects.

652 In the experimental tests, the algorithm was found to be a classifier of morphological surfaces  
653 since when there is no variation in morphology, the algorithm cannot classify the data, as  
654 occurred in the retablo test. Furthermore, it is worth mentioning that, as shown in the results  
655 of tests E and F from the 3D mesh reconstruction, the absence of point sets does not imply a  
656 complete surface. As a result, a complete segmentation would yield better results for  
657 transformation into parametric objects. It was also demonstrated that the classification  
658 algorithm, previously implemented on surfaces more complex than those of traditional  
659 architectural shapes, entails a reduction in accuracy for small scales.

660 On the other hand, optimal values of the segmentation parameters were sought so that  
661 representative data for Mesh-to-BIM could be obtained with the smallest number of points.  
662 Testbeds were carried out from 100 to 600 points per square metre to determine the required  
663 segmentation point density for BIM. It was determined that the point spacing should be at  
664 least 6 cm and uniform over the entire surface of the objects. Therefore, the results of the  
665 automatic segmentation by the CANUPO algorithm are not optimal for parameterising  
666 architectural elements in a BIM environment. The reason lies in the lack of essential points in  
667 certain areas and the presence of excessive gaps caused by the non-classification of points.

668 One of the main issues of this classifier is that, in the testbed of the wooden door, the  
669 algorithm determined points that did not belong to that subset (false positives) and  
670 accordingly classified them outside the surface. This is when the BIM operator has to intervene  
671 to analyse and interpret the data. Nevertheless, the algorithm yielded positive data of scale  
672 proportionality. Regarding the third testbed, the results showed no classification subsets. The

673 aim was to segment the cross, but the uniformity of the points indicated that the algorithm  
674 was unable to perform such segmentation.

675 Future work will not only adapt this algorithm to improve its applicability efficiency but also  
676 conduct further research based on it to meet the requirements of integrating point sets into  
677 BIM. These requirements are the uniformity in the point dispersion (which is related to the  
678 resolution of the set) and that the decimation exceeds 85 % of the total number of source  
679 points. Besides, geometric and colourimetric segmentation can be combined to classify TLS  
680 and SfM point clouds, which are characterised by geometric and colourimetric features. The  
681 algorithm was developed to classify terrain, vegetation, or gravel, achieving a classification  
682 accuracy of 98% when separating vegetation from the soil. However, it was not possible to  
683 achieve the same performance for less complex architectural features without excessive  
684 roughness.

## 685 **References**

- 686 [1] C. Bolognesi, V. Caffi, Extration of Primitives and Objects from Hshapes, *International*  
687 *Archives of Photogrammetry, Remote Sensing and Spatial Information Sciences*. XLII-  
688 2/W9 (2019) 151–156. <https://doi.org/10.5194/isprs-archives-XLII-2-W9-151-2019>.
- 689 [2] S. Bruno, M. De Fino, F. Fatiguso, Historic Building Information Modelling: performance  
690 assessment for diagnosis-aided information modelling and management, *Automation in*  
691 *Construction*. 86 (2018) 256–276. <https://doi.org/10.1016/j.autcon.2017.11.009>.
- 692 [3] J.E. Nieto-Julián, L. Lara, J. Moyano, Implementation of a TeamWork-HBIM for the  
693 Management and Sustainability of Architectural Heritage, *Sustainability*. 13 (2021)  
694 2161. <https://doi.org/10.3390/su13042161>.
- 695 [4] M. Murphy, E. McGovern, S. Pavia, Historic Building Information Modelling - Adding  
696 intelligence to laser and image based surveys of European classical architecture, *ISPRS*  
697 *Journal of Photogrammetry and Remote Sensing*. 76 (2013) 89–102.  
698 <https://doi.org/10.1016/j.isprsjprs.2012.11.006>.
- 699 [5] R. Pierdicca, M. Paolanti, F. Matrone, M. Martini, C. Morbidoni, E.S. Malinverni, E.  
700 Frontoni, A.M. Lingua, Point Cloud Semantic Segmentation Using a Deep Learning  
701 Framework for Cultural Heritage, *Remote Sensing*. 12 (2020) 1005.  
702 <https://doi.org/10.3390/rs12061005>.
- 703 [6] G. Patrucco, F. Chiabrando, A. Dameri, L.T. Losè, Geomatic contribution for the  
704 restoration project of the valentino castle green room. from data acquisition to  
705 integrated documentation, *The International Archives of the Photogrammetry, Remote*  
706 *Sensing and Spatial Information Sciences*. XLIII-B2 (2020) 885–892.  
707 <https://doi.org/10.5194/isprs-archives-xliii-b2-2020-885-2020>.
- 708 [7] N. Brodu, D. Lague, 3D terrestrial lidar data classification of complex natural scenes  
709 using a multi-scale dimensionality criterion: Applications in geomorphology, *ISPRS*  
710 *Journal of Photogrammetry and Remote Sensing*. 68 (2012) 121–134.  
711 <https://doi.org/10.1016/j.isprsjprs.2012.01.006>.
- 712 [8] Daniel Girardeau-Montaut, D. CloudCompare: 3D point cloud and mesh processing  
713 software. Open Source Project 2016., (n.d.). <https://www.danielgm.net/index.php>  
714 (accessed May 9, 2019).
- 715 [9] MoBiVAP Research Croup, Reconstrucción 3D, in: *Reconstrucción 3D, 2013*: p. 15.  
716 <http://lfa.mobivap.uva.es/~cevic/wp-content/uploads/2015/01/preface02.pdf>.

- 717 [10] S.F. El-Hakim, J.A. Beraldin, M. Picard, G. Godin, Detailed 3D reconstruction of large-  
718 scale heritage sites with integrated techniques, *IEEE Computer Graphics and*  
719 *Applications*. 24 (2004) 21–29. <https://doi.org/10.1109/MCG.2004.1318815>.
- 720 [11] L. Gomes, O. Regina Pereira Bellon, L. Silva, 3D reconstruction methods for digital  
721 preservation of cultural heritage: A survey, *Pattern Recognition Letters*. 50 (2014) 3–14.  
722 <https://doi.org/10.1016/j.patrec.2014.03.023>.
- 723 [12] S. Ochmann, R. Vock, R. Klein, Automatic reconstruction of fully volumetric 3D building  
724 models from oriented point clouds, *ISPRS Journal of Photogrammetry and Remote*  
725 *Sensing*. 151 (2019) 251–262. <https://doi.org/10.1016/j.isprsjprs.2019.03.017>.
- 726 [13] M. Gaiani, B. Benedetti, F.I. Apollonio, Teorie per rappresentare e comunicare i siti  
727 archeologici attraverso modelli critici, *SCIRES-IT : SCientific RESearch and Information*  
728 *Technology*. 1 (2011) 33–70. <https://doi.org/10.2423/i22394303v1n2p33>.
- 729 [14] L. De Luca, P. Veron, M. Florenzano, Reverse engineering of architectural buildings  
730 based on a hybrid modeling approach, *Computers & Graphics*. 30 (2006) 160–176.  
731 <https://doi.org/10.1016/j.cag.2006.01.020>.
- 732 [15] A. Fryskowska, J. Stachelek, A no-reference method of geometric content quality  
733 analysis of 3D models generated from laser scanning point clouds for hBIM, *Journal of*  
734 *Cultural Heritage*. 34 (2018) 95–108. <https://doi.org/10.1016/J.CULHER.2018.04.003>.
- 735 [16] A.A. Fernández, E. Soria, L. Agustín, J. Alberto, A. Adrián, B. Ereño, E. Salvador, I. Jordán,  
736 E. Nieto, J.J. Moyano, J. Antonio Herráez, Y. Espinosa, J. Leache, A. Rafael, M.  
737 Talaverano, A. Mahillo, J. González, A. José, I. Murillo, F. Carlos, R. María, I. Sardón, D.  
738 De Autor, BIM aplicado al Patrimonio Cultural Coordinador del proyecto Coordinadores  
739 de los grupos de trabajo, 2018.  
740 [https://www.researchgate.net/profile/Juan\\_Nieto10/publication/330183791\\_BIM\\_apli](https://www.researchgate.net/profile/Juan_Nieto10/publication/330183791_BIM_aplicado_al_Patrimonio_Cultural_Documento_14_Guia_de_usuarios_BIM_Building_SMAR_T_Spain_Chapter/links/5c328768299bf12be3b3ed0d/BIM-aplicado-al-Patrimonio-Cultural-Documento-14-Guia)  
741 [cado\\_al\\_Patrimonio\\_Cultural\\_Documento\\_14\\_Guia\\_de\\_usuarios\\_BIM\\_Building\\_SMAR](https://www.researchgate.net/profile/Juan_Nieto10/publication/330183791_BIM_aplicado_al_Patrimonio_Cultural_Documento_14_Guia_de_usuarios_BIM_Building_SMAR_T_Spain_Chapter/links/5c328768299bf12be3b3ed0d/BIM-aplicado-al-Patrimonio-Cultural-Documento-14-Guia)  
742 [T\\_Spain\\_Chapter/links/5c328768299bf12be3b3ed0d/BIM-aplicado-al-Patrimonio-](https://www.researchgate.net/profile/Juan_Nieto10/publication/330183791_BIM_aplicado_al_Patrimonio_Cultural_Documento_14_Guia_de_usuarios_BIM_Building_SMAR_T_Spain_Chapter/links/5c328768299bf12be3b3ed0d/BIM-aplicado-al-Patrimonio-Cultural-Documento-14-Guia)  
743 [Cultural-Documento-14-Guia](https://www.researchgate.net/profile/Juan_Nieto10/publication/330183791_BIM_aplicado_al_Patrimonio_Cultural_Documento_14_Guia_de_usuarios_BIM_Building_SMAR_T_Spain_Chapter/links/5c328768299bf12be3b3ed0d/BIM-aplicado-al-Patrimonio-Cultural-Documento-14-Guia) (accessed January 7, 2020).
- 744 [17] V. Bagnolo, R. Argiolas, A. Cuccu, HBIM for archaeological sites: from SFM based survey  
745 to algorithmic modeling, *International Archives of the Photogrammetry, Remote*  
746 *Sensing and Spatial Information Sciences - ISPRS Archives*. XLII–2 (2019) 57–63.  
747 <https://doi.org/10.5194/isprs-archives-XLII-2-W9-57-2019>.
- 748 [18] H.M. Yilmaz, M. Yakar, S.A. Gulec, O.N. Dulgerler, Importance of digital close-range  
749 photogrammetry in documentation of cultural heritage, *Journal of Cultural Heritage*. 8  
750 (2007) 428–433. <https://doi.org/10.1016/j.culher.2007.07.004>.
- 751 [19] F. Chiabrando, M. Lo Turco, C. Santagati, Digital invasions: From point clouds to  
752 historical building object modeling (h-BOM) of a unesco WHL site, *International*  
753 *Archives of the Photogrammetry, Remote Sensing and Spatial Information Sciences -*  
754 *ISPRS Archives*. 42 (2017) 171–178. [https://doi.org/10.5194/isprs-archives-XLII-2-W3-](https://doi.org/10.5194/isprs-archives-XLII-2-W3-171-2017)  
755 [171-2017](https://doi.org/10.5194/isprs-archives-XLII-2-W3-171-2017).
- 756 [20] L. Klein, N. Li, B. Becerik-Gerber, Imaged-based verification of as-built documentation of  
757 operational buildings, *Automation in Construction*. 21 (2012) 161–171.  
758 <https://doi.org/10.1016/j.autcon.2011.05.023>.
- 759 [21] J. Moyano, J.E. Nieto-Julián, D. Bienvenido-Huertas, D. Marín-García, Validation of  
760 Close-Range Photogrammetry for Architectural and Archaeological Heritage: Analysis of  
761 Point Density and 3d Mesh Geometry, *Remote Sensing*. 12 (2020) 3571.

- 762 <https://doi.org/10.3390/rs12213571>.
- 763 [22] P. Tang, D. Huber, B. Akinci, R. Lipman, A. Lytle, Automatic reconstruction of as-built  
764 building information models from laser-scanned point clouds: A review of related  
765 techniques, *Automation in Construction*. 19 (2010) 829–843.  
766 <https://doi.org/10.1016/j.autcon.2010.06.007>.
- 767 [23] J.A.H. Tortosa, D.T. Fuentes, M.L. Cereceda, Y.S. Berrio, The façade of the church of  
768 nuestra señora de la asunción in biar (Spain): From point cloud to HBIM, *WIT*  
769 *Transactions on the Built Environment*. 169 (2017) 69–77.  
770 <https://doi.org/10.2495/BIM170071>.
- 771 [24] A. Baik, From point cloud to Jeddah Heritage BIM Nasif Historical House – case study,  
772 *Digital Applications in Archaeology and Cultural Heritage*. 4 (2017) 1–18.  
773 <https://doi.org/10.1016/J.DAACH.2017.02.001>.
- 774 [25] J. Jung, S. Hong, S. Jeong, S. Kim, H. Cho, S. Hong, J. Heo, Productive modeling for  
775 development of as-built BIM of existing indoor structures, *Automation in Construction*.  
776 42 (2014) 68–77. <https://doi.org/10.1016/j.autcon.2014.02.021>.
- 777 [26] X. Yang, P. Grussenmeyer, M. Koehl, H. Macher, A. Murtiyoso, T. Landes, Review of built  
778 heritage modelling: Integration of HBIM and other information techniques, *Journal of*  
779 *Cultural Heritage*. 46 (2020) 350–360. <https://doi.org/10.1016/j.culher.2020.05.008>.
- 780 [27] S. Spina, K. Debattista, K. Bugeja, A. Chalmers, Point Cloud Segmentation for Cultural  
781 Heritage Sites, *VAST: International Symposium on Virtual Reality, Archaeology and*  
782 *Intelligent Cultural Heritage*. (2011) 41–48. [https://doi.org/10.2312/VAST/VAST11/041-](https://doi.org/10.2312/VAST/VAST11/041-048)  
783 [048](https://doi.org/10.2312/VAST/VAST11/041-048).
- 784 [28] H. Macher, T. Landes, P. Grussenmeyer, From point clouds to building information  
785 models: 3D semi-automatic reconstruction of indoors of existing buildings, *Applied*  
786 *Sciences (Switzerland)*. 7 (2017) 1–30. <https://doi.org/10.3390/app7101030>.
- 787 [29] E. Grilli, F. Menna, F. Remondino, A review of point clouds segmentation and  
788 classification algorithms., *The International Archives of the Photogrammetry, Remote*  
789 *Sensing and Spatial Information Sciences*. XLII-2/W3 (2017) 340–344.  
790 <https://doi.org/10.5194/isprs-archives-XLII-2-W3-339-2017>.
- 791 [30] S. Pu, G. Vosselman, Knowledge based reconstruction of building models from  
792 terrestrial laser scanning data, *ISPRS Journal of Photogrammetry and Remote Sensing*.  
793 64 (2009) 575–584. <https://doi.org/10.1016/j.isprsjprs.2009.04.001>.
- 794 [31] F. Boochs, A. Marbs, H. Hmida, H. Truong, A. Karmachaiya, C. Cruz, A. Habed, C. Nicolle,  
795 Y. Voisin, Integration of knowledge to support automatic object reconstruction from  
796 images and 3D data, in: *Eighth International Multi-Conference on Systems, Signals &*  
797 *Devices*, Institute of Electrical and Electronics Engineers (IEEE), 2011: pp. 1–13.  
798 <https://doi.org/10.1109/ssd.2011.5993558>.
- 799 [32] X. Lu, A.K. Jain, D. Colbry, Matching 2.5D face scans to 3D models, *IEEE Transactions on*  
800 *Pattern Analysis and Machine Intelligence*. 28 (2006) 31–42.  
801 <https://doi.org/10.1109/TPAMI.2006.15>.
- 802 [33] S. Ochmann, R. Vock, R. Wessel, R. Klein, Automatic reconstruction of parametric  
803 building models from indoor point clouds, *Computers & Graphics*. 54 (2016) 94–103.  
804 <https://doi.org/10.1016/J.CAG.2015.07.008>.
- 805 [34] S. Hong, J. Jung, S. Kim, H. Cho, J. Lee, J. Heo, Semi-automated approach to indoor

- 806 mapping for 3D as-built building information modeling, *Computers, Environment and*  
807 *Urban Systems*. 51 (2015) 34–46.  
808 <https://doi.org/10.1016/J.COMPENVURBSYS.2015.01.005>.
- 809 [35] C. Thomson, J. Boehm, Automatic geometry generation from point clouds for BIM,  
810 *Remote Sensing*. 7 (2015) 11753–11775. <https://doi.org/10.3390/rs70911753>.
- 811 [36] T. Rabbani, F.A. Van Den Heuvel, G. Vosselman, Segmentation of point clouds using  
812 smoothness constraint, *International Archives of the Photogrammetry, Remote Sensing*  
813 *and Spatial Information Sciences - ISPRS Archives*. 36 (2006) 248–253.  
814 [https://doi.org/http://www.isprs.org/proceedings/XXXVI/part5/paper/RABB\\_639.pdf](https://doi.org/http://www.isprs.org/proceedings/XXXVI/part5/paper/RABB_639.pdf).
- 815 [37] M.A. Wani, H.R. Arabnia, Parallel edge-region-based segmentation algorithm targeted  
816 at reconfigurable MultiRing network, *Journal of Supercomputing*. 25 (2003) 43–62.  
817 <https://doi.org/10.1023/A:1022804606389>.
- 818 [38] M.A. Fischler, R.C. Bolles, RANSAC1981.pdf, *Graphics and Image Processing*. 24 (1981)  
819 381–395. <https://doi.org/10.1145/358669.358692>.
- 820 [39] M. Andriasyan, J. Moyano, J.E. Nieto-Julián, D. Antón, From Point Cloud Data to Building  
821 Information Modelling: An Automatic Parametric Workflow for Heritage, *Remote*  
822 *Sensing 2020*, Vol. 12, Page 1094. 12 (2020) 1094.  
823 <https://doi.org/10.3390/RS12071094>.
- 824 [40] D. Antón, B. Medjdoub, R. Shrahily, J. Moyano, Accuracy evaluation of the semi-  
825 automatic 3D modeling for historical building information models, *International Journal*  
826 *of Architectural Heritage*. 12 (2018) 790–805.  
827 <https://doi.org/10.1080/15583058.2017.1415391>.
- 828 [41] L. Barazzetti, Parametric as-built model generation of complex shapes from point  
829 clouds, *Advanced Engineering Informatics*. 30 (2016) 298–311.  
830 <https://doi.org/10.1016/j.aei.2016.03.005>.
- 831 [42] C. Dore, M. Murphy, Semi-Automatic Generation of As- Built Bim Façade Geometry  
832 From Laser and Image Data, *Journal of Information Technology in Construction*. 19  
833 (2014) 20–46. <http://www.itcon.org/2014/2>.
- 834 [43] M. Zheliazkova, R. Naboni, I. Paoletti, A parametric-assisted method for 3D generation  
835 of as-built BIM models for the built heritage, in: *Structural Studies, Repairs and*  
836 *Maintenance of Heritage Architecture XIV*, WIT Press, 2015: pp. 693–704.  
837 <https://doi.org/10.2495/str150581>.
- 838 [44] B. Rivera, P. Merchán, S. Salamanca, E. Pérez, M.D. Moreno, M.J. Merchán, Creación de  
839 bibliotecas de objetos paramétricos para su integración en modelo HBIM, in: *Actas de*  
840 *Las XXXIX Jornadas de Automática*, Badajoz, 5-7 de Septiembre de 2018, 2018: pp.  
841 1069–1076. <http://hdl.handle.net/10662/8883>.
- 842 [45] K. Aitelkadi, D. Tahiri, E. Simonetto, I. Sebari, L. Polidori, Segmentation of heritage  
843 building by means of geometric and radiometric components from terrestrial laser  
844 scanning, *ISPRS Annals of the Photogrammetry, Remote Sensing and Spatial*  
845 *Information Sciences*. 2 (2013) 1–6. <https://doi.org/10.5194/isprsannals-II-5-W1-1-2013>.
- 847 [46] S. Gonizzi Barsanti, G. Guidi, L. De Luca, Segmentation of 3D models for cultural  
848 heritage structural analysis - some critical some issues, *ISPRS Annals of the*  
849 *Photogrammetry, Remote Sensing and Spatial Information Sciences*. 4 (2017) 115–122.

- 850 <https://doi.org/10.5194/isprs-annals-IV-2-W2-115-2017>.
- 851 [47] P.C. Library, Point Cloud Library | The Point Cloud Library (PCL) is a standalone, large  
852 scale, open project for 2D/3D image and point cloud processing., (2020).  
853 <https://pointclouds.org/> (accessed January 7, 2021).
- 854 [48] H. Ding, X. Jiang, B. Shuai, A.Q. Liu, G. Wang, Semantic Segmentation with Context  
855 Encoding and Multi-Path Decoding, *IEEE Transactions on Image Processing*. 29 (2020)  
856 3520–3533. <https://doi.org/10.1109/TIP.2019.2962685>.
- 857 [49] G.I. Penagos-Londoño, C. Rodriguez-Sanchez, F. Ruiz-Moreno, E. Torres, A machine  
858 learning approach to segmentation of tourists based on perceived destination  
859 sustainability and trustworthiness, *Journal of Destination Marketing and Management*.  
860 19 (2021) 100532. <https://doi.org/10.1016/j.jdmm.2020.100532>.
- 861 [50] J. Llamas, P. M. Lerones, R. Medina, E. Zalama, J. Gómez-García-Bermejo, Classification  
862 of Architectural Heritage Images Using Deep Learning Techniques, *Applied Sciences*. 7  
863 (2017) 992. <https://doi.org/10.3390/app7100992>.
- 864 [51] E.-K. Stathopoulou, F. Remondino, Semantic photogrammetry -Boosting image-based  
865 3D reconstruction with semantic labeling., *ISPRS - International Archives of the  
866 Photogrammetry, Remote Sensing and Spatial Information Sciences*. XLII-2/W9 (2019)  
867 685–690. <https://doi.org/10.5194/isprs-archives-XLII-2-W9-685-2019>.
- 868 [52] Z. Wu, S. Song, A. Khosla, Y. Fisher, L. Zhang, X. Tang, J. Xiao, 3D ShapeNets: A Deep  
869 Representation for Volumetric Shapes, 2015. <http://3dshapenets.cs.princeton.edu>  
870 (accessed February 10, 2021).
- 871 [53] C.R. Qi, H. Su, K. Mo, L.J. Guibas, PointNet: Deep learning on point sets for 3D  
872 classification and segmentation, in: *Proceedings - 30th IEEE Conference on Computer  
873 Vision and Pattern Recognition, CVPR 2017*, Institute of Electrical and Electronics  
874 Engineers Inc., 2017: pp. 77–85. <https://doi.org/10.1109/CVPR.2017.16>.
- 875 [54] N. Oses, F. Dornaika, A. Moujahid, Image-Based Delineation and Classification of Built  
876 Heritage Masonry, *Remote Sensing*. 6 (2014) 1863–1889.  
877 <https://doi.org/10.3390/rs6031863>.
- 878 [55] G. Bitelli, G. Castellazzi, A.M. D'altri, S. De Miranda, A. Lambertini, I. Selvaggi,  
879 Automated voxel model from point clouds for structural analysis of cultural heritage, in:  
880 *International Archives of the Photogrammetry, Remote Sensing and Spatial Information  
881 Sciences - ISPRS Archives, International Society for Photogrammetry and Remote  
882 Sensing*, 2016: pp. 191–197. <https://doi.org/10.5194/isprsarchives-XLI-B5-191-2016>.
- 883 [56] T. Hinks, H. Carr, L. Truong-Hong, D.F. Laefer, Point Cloud Data Conversion into Solid  
884 Models via Point-Based Voxelization, *Journal of Surveying Engineering*. 139 (2013) 72–  
885 83. [https://doi.org/10.1061/\(asce\)su.1943-5428.0000097](https://doi.org/10.1061/(asce)su.1943-5428.0000097).
- 886 [57] M. Rouse, ¿Qué es vóxel? - Definición de WhatIs.com, (2015).  
887 <https://whatis.techtarget.com/definicion/voxel> (accessed February 10, 2021).
- 888 [58] C. Wang, Y.K. Cho, C. Kim, Automatic BIM component extraction from point clouds of  
889 existing buildings for sustainability applications, *Automation in Construction*. 56 (2015)  
890 1–13. <https://doi.org/10.1016/j.autcon.2015.04.001>.
- 891 [59] M. Ye, S. Xu, T. Cao, HVNet: Hybrid Voxel Network for LiDAR Based 3D Object Detection,  
892 in: *Proceedings of the IEEE Computer Society Conference on Computer Vision and  
893 Pattern Recognition*, IEEE Computer Society, 2020: pp. 1628–1637.

- 894 <https://doi.org/10.1109/CVPR42600.2020.00170>.
- 895 [60] Q. Lu, S. Lee, Image-Based Technologies for Constructing As-Is Building Information  
896 Models for Existing Buildings, *Journal of Computing in Civil Engineering*. 31 (2017)  
897 04017005. [https://doi.org/10.1061/\(asce\)cp.1943-5487.0000652](https://doi.org/10.1061/(asce)cp.1943-5487.0000652).
- 898 [61] J. Moyano, J.E. Nieto-Julián, D. Antón, E. Cabrera, D. Bienvenido-Huertas, N. Sánchez,  
899 Suitability Study of Structure-from-Motion for the Digitisation of Architectural  
900 (Heritage) Spaces to Apply Divergent Photograph Collection, *Symmetry*. 12 (2020) 1981.  
901 <https://doi.org/10.3390/sym12121981>.
- 902 [62] A. Osello, The future of drawing with BIM for Engineers and Architects -, Dario Flaccovio  
903 Editore Srl. (2012).  
904 [https://scholar.google.es/scholar?hl=es&as\\_sdt=0%2C5&q=The+future+of+drawing+with+BIM+for+Engineers+and+Architects&btnG=](https://scholar.google.es/scholar?hl=es&as_sdt=0%2C5&q=The+future+of+drawing+with+BIM+for+Engineers+and+Architects&btnG=) (accessed March 10, 2021).  
905
- 906 [63] L. Weidner, G. Walton, R. Kromer, Classification methods for point clouds in rock slope  
907 monitoring: A novel machine learning approach and comparative analysis, *Engineering*  
908 *Geology*. 263 (2019) 105326. <https://doi.org/10.1016/j.enggeo.2019.105326>.
- 909 [64] L.J. Sánchez-Aparicio, S. Del Pozo, L.F. Ramos, A. Arce, F.M. Fernandes, Heritage site  
910 preservation with combined radiometric and geometric analysis of TLS data,  
911 *Automation in Construction*. 85 (2018) 24–39.  
912 <https://doi.org/10.1016/j.autcon.2017.09.023>.
- 913 [65] Ľ. Kovanič, P. Blistan, R. Urban, M. Štroner, K. Pukanská, K. Bartoš, J. Palková, Analytical  
914 determination of geometric parameters of the rotary kiln by novel approach of tls point  
915 cloud segmentation, *Applied Sciences (Switzerland)*. 10 (2020) 1–27.  
916 <https://doi.org/10.3390/app10217652>.
- 917 [66] Z. Li, L. Zhang, P.T. Mathiopoulos, F. Liu, L. Zhang, S. Li, H. Liu, A hierarchical  
918 methodology for urban facade parsing from TLS point clouds, *ISPRS Journal of*  
919 *Photogrammetry and Remote Sensing*. 123 (2017) 75–93.  
920 <https://doi.org/10.1016/j.isprsjprs.2016.11.008>.
- 921 [67] C. Paris, D. Kelbe, J. Van Aardt, L. Bruzzone, A Novel Automatic Method for the Fusion  
922 of ALS and TLS LiDAR Data for Robust Assessment of Tree Crown Structure, *IEEE*  
923 *Transactions on Geoscience and Remote Sensing*. 55 (2017) 3679–3693.  
924 <https://doi.org/10.1109/TGRS.2017.2675963>.
- 925 [68] A. Burt, M. Disney, K. Calders, Extracting individual trees from lidar point clouds using  
926 *treeseg*, *Methods in Ecology and Evolution*. 10 (2018) 2041–210X.13121.  
927 <https://doi.org/10.1111/2041-210X.13121>.
- 928 [69] F. Bosché, M. Ahmed, Y. Turkan, C.T. Haas, R. Haas, The value of integrating Scan-to-  
929 BIM and Scan-vs-BIM techniques for construction monitoring using laser scanning and  
930 BIM: The case of cylindrical MEP components, *Automation in Construction*. 49 (2015)  
931 201–213. <https://doi.org/10.1016/j.autcon.2014.05.014>.
- 932 [70] Q. Wang, J. Guo, M.-K. Kim, An Application Oriented Scan-to-BIM Framework, *Remote*  
933 *Sensing*. 11 (2019) 365. <https://doi.org/10.3390/rs11030365>.
- 934 [71] J. Moyano, C.P. Odriozola, J.E. Nieto-Julián, J.M. Vargas, J.A. Barrera, J. León, Bringing  
935 BIM to archaeological heritage: Interdisciplinary method/strategy and accuracy applied  
936 to a megalithic monument of the Copper Age, *Journal of Cultural Heritage*. (2020).  
937 <https://doi.org/10.1016/j.culher.2020.03.010>.



- 938 [72] L. Ma, R. Favier, L. Do, E. Bondarev, P.H.N. De With, Plane segmentation and decimation  
939 of point clouds for 3D environment reconstruction, in: 2013 IEEE 10th Consumer  
940 Communications and Networking Conference, CCNC 2013, IEEE, 2013: pp. 43–49.  
941 <https://doi.org/10.1109/CCNC.2013.6488423>.
- 942 [73] X. Yang, Y.-C. Lu, A. Murtiyoso, M. Koehl, P. Grussenmeyer, HBIM Modeling from the  
943 Surface Mesh and Its Extended Capability of Knowledge Representation, *Isprs Int. J.*  
944 *Geo-Inf.* 8 (2019) 301. <https://doi.org/10.3390/ijgi8070301>.
- 945 [74] M. Kazhdan, H. Hoppe, Screened poisson surface reconstruction, *ACM Transactions on*  
946 *Graphics.* 32 (2013) 1–13. <https://doi.org/10.1145/2487228.2487237>.
- 947 [75] S. Logothetis, E. Stylianidis, BIM Open Source Software (OSS) for the documentation of  
948 cultural heritage, *Virtual Archaeology Review.* 7 (2016) 28.  
949 <https://doi.org/10.4995/var.2016.5864>.
- 950 [76] D. Falk-Petersen, openBIM - buildingSMART International, (2018).  
951 <https://www.buildingsmart.org/about/openbim/> (accessed June 14, 2021).
- 952 [77] J. Moyano, J.E. Nieto-Julián, L.M. Lenin, S. Bruno, Operability of Point Cloud Data in an  
953 Architectural Heritage Information Model, *International Journal of Architectural*  
954 *Heritage.* (2021). <https://doi.org/10.1080/15583058.2021.1900951>.
- 955 [78] BIMserver, BIMserver.org – Open source building information server, (2021).  
956 <https://bimserver.org/> (accessed June 14, 2021).
- 957 [79] D.S. Oasis, IFCWebServer – Open BIM Server and Online BIMViewer, (n.d.).  
958 <https://ifcwebserver.org/> (accessed June 14, 2021).
- 959 [80] F. Diara, F. Rinaudo, Open source hbim for cultural heritage: A project proposal, in:  
960 *International Archives of the Photogrammetry, Remote Sensing and Spatial Information*  
961 *Sciences - ISPRS Archives, International Society for Photogrammetry and Remote*  
962 *Sensing,* 2018: pp. 303–309. <https://doi.org/10.5194/isprs-archives-XLII-2-303-2018>.
- 963 [81] I. Nishanbaev, A web repository for geo-located 3D digital cultural heritage models,  
964 *Digital Applications in Archaeology and Cultural Heritage.* 16 (2020) e00139.  
965 <https://doi.org/10.1016/j.daach.2020.e00139>.

966